Probing Fluorinated Motifs onto Dual AChE–MAO B Inhibitors: Rational Design, Synthesis, Biological Evaluation and Early-ADME Studies

Mariagrazia Rullo,[1] Marco Cipolloni,[2] Marco Catto,[1] Carolina Colliva,[2] Daniela Valeria Miniero,[3] Tiziana Latronico,[3] Modesto de Candia,[1] Tiziana Benicchi,[2] Anna Linusson,[4] Nicola Giacchè,[2] Cosimo Damiano Altomare,[1] Leonardo Pisani[1,*]

[1] Department of Pharmacy- Pharmaceutical Sciences, University of Bari "Aldo Moro", via Orabona 4, 70125-Bari, Italy
[2] TES Pharma s.r.l., Corso Vannucci 47, 06121, Perugia, Italy
[3] Department of Biosciences, Biotechnologies and Biopharmaceutics, University of Bari "Aldo Moro", via Orabona, 4, 70125-Bari, Italy
[4] Department of Chemistry, Umeå University, 90187, Umeå, Sweden

Abstract

Bioisosteric H/F or CH_2OH/CF_2H replacement was introduced in coumarin derivatives previously characterized as dual AChE-MAO B inhibitors to probe the effects on both inhibitory potency and drug-likeness. Along with in vitro screening, we investigated early-ADME parameters related to solubility and lipophilicity ($Sol_{7.4}$, $CHI_{7.4}$, $LogD_{7.4}$), oral bioavailability and CNS-penetration (PAMPA-HDM and PAMPA-BBB assays, Caco-2 bidirectional transport study), metabolic liability (half-lives and clearance in microsomes, inhibition of CYP3A4). Both specific and non-specific tissue toxicity were determined in SH-SY5Y and HepG2 lines, respectively. Compound **15** bearing a $-CF_2H$ motif emerged as a water-soluble, orally bioavailable CNS-permeant potent inhibitor of both human AChE (IC_{50} = 550 nM) and MAO B (IC_{50} = 8.2 nM, B/A selectivity > 1200). Moreover, **15** behaved as safe and metabolically stable neuroprotective agent against H_2O_2 and NMDA insults, devoid of cytochrome liability.

Keywords: fluorine, isosteres, coumarin, multitargeting ligands, monoamine oxidases, cholinesterases, ADME

Introduction

As life-expectancy is getting higher, the global impact of age-related diseases increases its burden on the socio-economic cost for care-giving.[1] More than 50 million people live with dementia worldwide, mostly associated to Alzheimer's disease (AD).[2,3] Unfortunately, these figures are predicted to more than triple by next two decades, unless real effective treatments become available to clinicians. Huge efforts devoted to the comprehension of AD[4] mapped a multifactorial landscape enrolling much more than 100 mechanisms continuously enriched within the Aetionomy project.[5] Despite great improvement scored in disease knowledge and understanding, effective therapies are still elusive also as the consequence of lacking unique druggable etiological event.[6] After memantine (Chart 1), a glutamate NMDA-receptor blocker able to improve language and memory skills approved by EMA (2002) and FDA (2003), no more drug has joined the toolbox for AD therapy with the exception of an amyloid-directed monoclonal antibody, aducanumab. Therefore, the cornerstone of Alzheimer's treatment is still occupied by three acetylcholinesterase (AChE) inhibitors (Chart 1; rivastigmine, galantamine, donepezil),[7] able to control symptoms in the early stage of the disease without preventing nor delaying neurotoxic cascade ultimately fatal.[8] The high failure rate associated to adverse outcomes for most phase II/III clinical trials[9] discouraged massive investment in the field, draining resources progressively away from AD research. At present, the drug development pipeline counts more than 100 different agents showing diverse mechanism of action, always more frequently distancing amyloid cascade.[10]

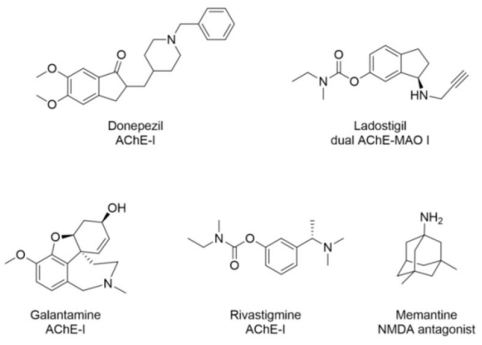

Chart 1. Small molecules approved by FDA or under clinical trials for AD treatment.

The urgent need for disease-modifying therapies encouraged researchers to devise alternatives to single-targeting molecules along cutting-edge multitarget strategies.[11] Already successfully applied to the treatment of cancer and cardiovascular diseases, polypharmacology protocols rooted on drug cocktails or fixed-dose combinations of active ingredients provide the control of symptoms and halt/delay the progression of such complex multifactorial diseases. As a particular case of polypharmacology, according to definitions, multi-target directed ligands (MTDLs) or designed multiple ligands (DMLs) stand for single molecular entities intentionally designed to modulate simultaneously two or more targets relevant for disease pathogenesis. The combination of biochemical mechanisms might rise the hope for a real disease-modifying effect thanks to synergic or additive activities. To this extent, the right choice of networked biological targets is a major concern. More recently, different combinations of targets (dual 5-HT_4R partial agonism / AChE inhibition,[12] H3R antagonism / VGCC blockade,[13] GSK-3α/β inhibition / AChE inhibition,[14] NMDAR binding / AChE inhibition,[15] A_1/A_{2A}ARs blockade / MAO B inhibition,[16] AChE inhibition / MAO inhibition / H3R antagonism,[17] among others) have been addressed as potential druggable options to treat AD with the use of multipotent small molecules. However, the old-fashioned dual inhibition of acetylcholinesterase (AChE) and monoamine oxidases (MAOs) is still an appealing research field[18–24] after the launch of ladostigil (Chart 1),[25] a dual irreversible inhibitor currently in clinical trials against mild cognitive imparment.[26] The blockade of AChE activity contributes an increased neurotransmitter level to counteract the depletion of cholinergic tone. Moreover, the occupancy of peripheral anionic subsite (PAS) with dual binding site AChE inhibitors can mitigate β-amyloid aggregation rate.[27] On the other side, brain MAO activity increases with ageing[28] and in cortex and hippocampus of AD patients,[29,30] thus, its inhibition can mitigate ROS production, in particular limiting hazardous species deriving from aldehydes and H_2O_2 produced as catalytic cycle by-products.

After having largely explored the decoration of 2*H*-chromen-2-one as privileged-scaffold to develop potent dual AChE-MAO B inhibitors,[18,19,31,32] in the present work we aimed at probing the

effect of fluorinated motifs on both in vitro potency and drug-like features of multimodal hit compounds already developed by us as potential agents against neurodegenerative disorders.

Despite being slightly larger than hydrogen (van der Waals radius = 1.2 Å), covalently bound fluorine (1.47 Å) could strongly impact molecular properties of drugs and drug-like hit compounds as well. Since the early 1980s, the presence of fluorinated molecules has become routinely observed among newly marketed synthetic drugs.[33] Most properties raise from the highest electronegativity in the Pauling scale attributed to F (3.98), which could modulate pK_a of nearby functional groups, increase the stability of proximal C-H bonds prone to oxidation, and affect binding energies with macromolecule targets by contributing direct multipolar contacts and/or affecting indirect dipolar interactions.[34] H/F exchange is most often envisaged to mitigate hepatic clearance and achieve higher bioavailability, particularly for orally administered drugs suffering from first-pass metabolism employing CYP enzymatic machineries.[35] To this extent, aromatic H/F isosteric mimicry is often pursued with the aim of decreasing C-H oxidation rates leading to *para*-hydroxylation without producing significant changes in binding free energies because of the size of F atom, rarely involved in steric clashes, and small contributions brought by lipophilic interactions (van der Waals, dipolar), provided that direct binding contacts with F and repulsive interactions are absent. Apart from (per)fluorinated alkanes, the introduction of F atom(s) increases the lipophilicity of parent compounds thus affecting physicochemical properties (solubility, membrane permeability) and related pharmacokinetics (metabolic liabilities, non-specific activities, target distribution).[36] Ultimately successful drug discovery programs result from well-balancing all of these parameters. Indeed, fluorinated bioisosteres represent a useful, rapidly expanding tactic in medicinal chemistry useful to control target potency/selectivity, solubility, conformational bias, pK_a, and temper metabolism, off-target distribution, bioavailability.

Herein we employed fluorinated motifs to decorate diverse 2*H*-chromen-2-ones, previously reported as dual AChE-MAO B hits by some of us.[18,31,32] Apart from H/F exchange on phenyl rings,

the replacement of primary alcohols with difluoromethyl groups (CF_2H) as weaker hydrogen bonding (HB) donor bioisosteres was investigated (Figure 1).[37] CF_2H groups make compounds more lipophilic than OH while maintaining HB ability though with lower acidity.[38] Given that F-motifs might deeply impact drug-likeness, after in vitro biological evaluations toward target enzymes (ChEs and MAOs), the most interesting compounds were prioritized to assess physicochemical properties (solubility, lipophilicity, $logD_{7.4}$, membrane permeability) that are relevant for hit finding. Preliminarily, early-ADME profiling enclosed metabolic liability, brain penetration and inherent cytotoxicity determination. In light of potent in vitro inhibitory data, non-fluorinated analogues were enrolled in drug-likeness study, too.

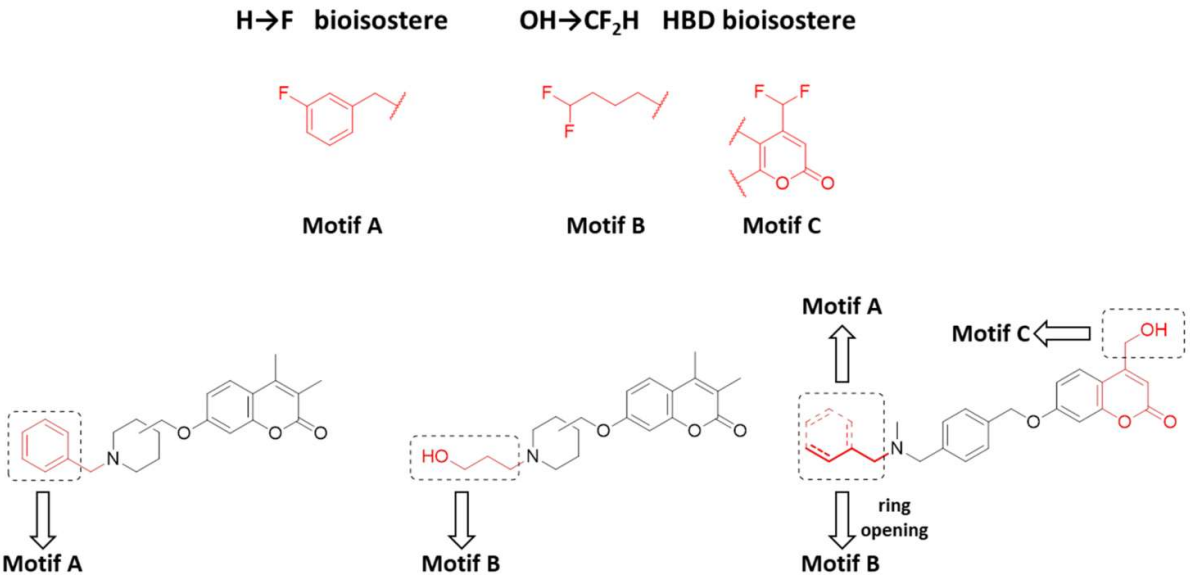

Figure 1. Rational design of fluorinated (bio)isosteres.

Synthesis

The preparation of difluoromethyl compounds required the synthesis of a common intermediate (**1d**) as illustrated in Scheme 1.[39] Commercially available 1,4-butanediol was mono-protected as benzoate followed by PCC-mediated oxidation of **1a**. The nucleophilic fluorination of aldehyde **1b** was accomplished by DAST yielding benzoate **1c**, that was in turn transformed into nosylate **1d**, as

a better leaving group, by applying a two-steps methanolysis/nosylation protocol. Nucleophilic substitution reactions coupling the suitable piperidine **2a-b**[31] with **1d** or suitable benzyl bromide as the electrophilic partner provided final compounds **3-7** (Scheme 2).

Scheme 1. Synthesis of gem-difluorointermediate **1d**

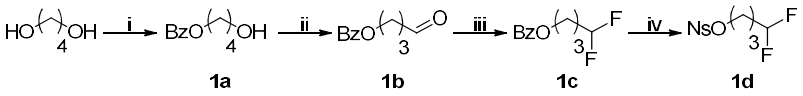

Reagents and conditions: i) benzoyl chloride, DIEA, acetonitrile, room temperature, 3 h; ii) PCC, celite, an. CH_2Cl_2, room temperature, 21 h; iii) DAST, an. CH_2Cl_2, 0 °C to room temperature, 1 h; iv) a) $NaOCH_3$, TFA, methanol, room temperature, 1.5 h; b) NsCl, TEA, DMAP, an. CH_2Cl_2, room temperature, 1.5 h.

Scheme 2. Synthesis of piperidines **3-7**

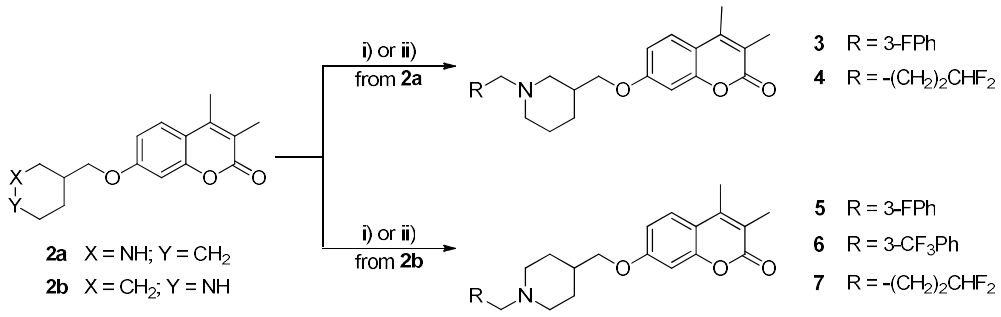

Reagents and conditions: i) for **(±)-3**, **5**, **6**: suitable benzyl bromide, K_2CO_3, acetonitrile, Δ, 5 h; ii) for **(±)-4** and **7**: **1d**, K_2CO_3, acetonitrile, 80 °C, 18 h, sealed vessel.

As indicated in Scheme 3, appropriate halides **9b-d** were reacted with excess methylamine yielding **12a-c** prior to final alkylation with **1d** to afford coumarins **13-15**. Compounds **10**, **11** and **16** were obtained by heating intermediate bromides **9a-b** with suitable 3-F-substituted amine **8a-c** in refluxing acetonitrile or under microwave irradiation to afford desired difluoromethyl-derivatives.

Scheme 3. Synthesis of benzylamines **10, 11, 13-16**

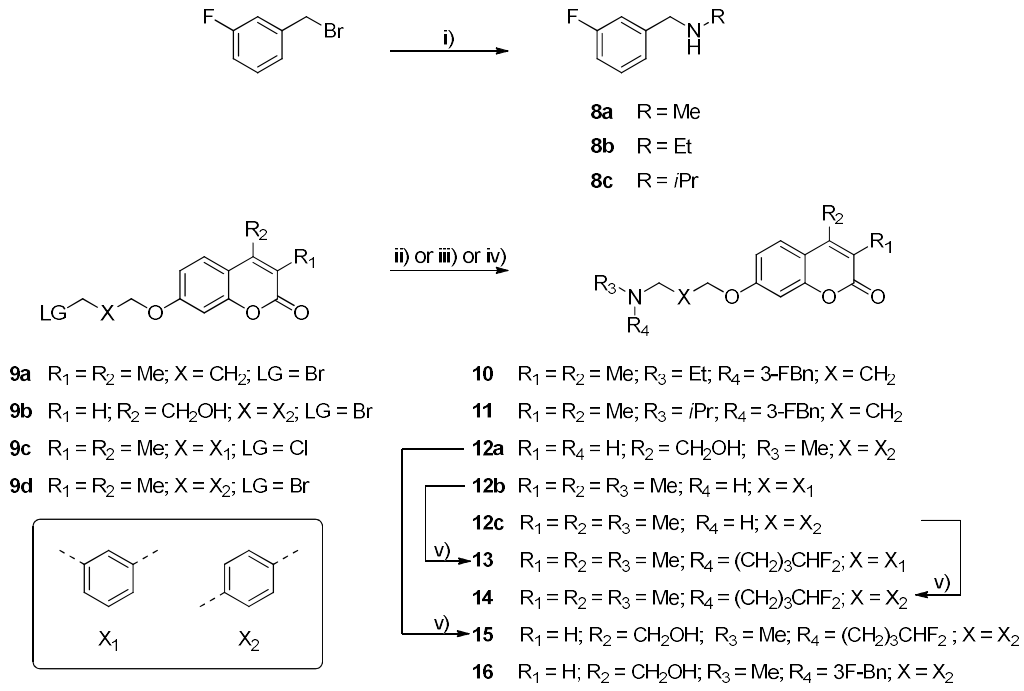

Reagents and conditions: i) CH_3NH_2 (for **8a**) or $CH_3CH_2NH_2$ (for **8b**) or $(CH_3)_2CHNH_2$ (for **8c**), THF, room temperature, 6 h; ii) for **10-11** (from **9a**): **8b** (for **10**) or **8c** (for **11**), K_2CO_3, KI (cat.), acetonitrile, Δ, 10 h; iii) for **12a** (from **9b**), **12b** (from **9c**), **12c** (from **9d**): CH_3NH_2, THF, room temperature, 18 h; iv) for **16** (from **9b**): **8a**, K_2CO_3, KI (cat.), acetonitrile, 130 °C, 30 min, MW; v) **1d**, K_2CO_3, acetonitrile, 80 °C, 18 h, sealed vessel.

Scheme 4 illustrates the synthetic pathway leading to **19**. The procedure started from the controlled oxidation of alcohol **17** to aldehyde **18** in the presence of activated MnO_2 followed by DAST-promoted fluorination giving final compound **19**.

Scheme 4. Synthesis of coumarin **19**

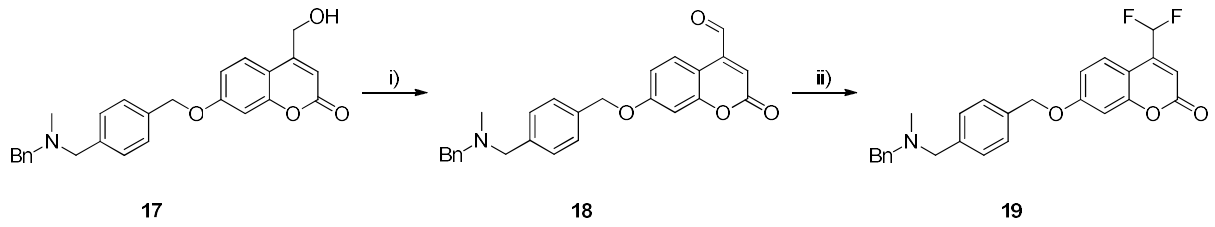

Reagents and conditions: i) MnO_2, an. CH_2Cl_2, room temperature, 2 h; ii) DAST, an. CH_2Cl_2, 0 °C to room temperature, overnight.

Structure-activity relationships

All coumarin derivatives in Table 1 were evaluated in vitro as inhibitors of target enzymes (hMAOs, hAChE, hsBChE) by applying kinuramine and Ellmann's assay[40] for MAOs[18] and ChEs,[41] respectively. Regarding activity toward MAO isoenzymes, we aimed at achieving B/A selectivity to avoid well-known side-effects linked to the inhibition of peripheral MAO A, termed "cheese effect" from hypertensive crisis after tyramine-rich food consumption.[42] On the other side, non-selective AChE inhibition represented an appealing feature due to the increasing evidence highlighting the expedient BChE activity[43] targeting in AD brains.

Since H/F substitution on aromatic rings could negatively affect solubility, we preferred to study only *meta*-positions which could somehow disrupt symmetry and induce a lower lipophilicity penalty compared to more symmetric *para*-derivatives. As inferred by in vitro inhibitory data obtained for *N*-benzylpiperidines **(±)-3**, **5**, **(±)-21** and **23**, the introduction of F-atom at the *meta*-position of phenyl rings exerted a negligible impact on activity (MAO B IC_{50}: from moderate to low nanomolar; AChE IC_{50}: from low micromolar to submicromolar) while increasing molecular lipophilicity. More interestingly, the presence of *m*-F substitution did not alter inhibitory trends markedly. With the exception of chiral samples, whose MAO B inhibition was slightly enhanced by H/F exchange (IC_{50} for **(±)-3** = 12 nM, IC_{50} for **(±)-21** = 30 nM), in all cases inhibitory activities were equipotent or slightly worsened on both targets (compare **(±)-3** with **(±)-21**, **5** with **23**). Moreover, the CF_3-motif installed on compound **6** was unable to improve binding interactions with MAO B as well as AChE. Open chain derivatives **10**-**11** were designed to remove chirality issues from analogue **(±)-3**. Ethyl-substituted **10** was a better MAO B inhibitor than *i*Pr-derivative **11** (IC_{50} = 73 nM and 350 nM, respectively), both being less active than parent chiral compound **(±)-3**. On the other side, AChE inhibition was not affected by piperidine ring-opening and **(±)-3**, **10**-**11** showed close low-micromolar IC_{50} values, which returned better-balanced bioactivity profiles as dual inhibitors than **(±)-3**. Looking at bis-benzylamine, F-introduction in **16** was not tolerated by AChE enzymatic cavity (IC_{50} = 330 nM) and produced a 3-fold activity drop (**17**, IC_{50} = 120 nM)

whereas MAO B inhibition remained untouched (IC_{50} = 10 nM). Notwithstanding, **16**-**17** were among the most interesting samples of the whole series showing nanomolar dual-inhibitory potencies toward AChE and MAO B, micromolar BChE inhibition and noteworthy B/A selectivity (SI > 1000).

Alcohol bioisosteric replacement based on CF_2H as lipophilic hydrogen bonding donor produced a different activity trend in chiral (**(±)-4** vs. **(±)-20**) and achiral analogue (**7** vs. **22**) pairs, the latter showing close inhibitory potencies. A more remarkable effect was retrieved upon comparing racemic **4** and **20**, since CF_2H-group improved MAO B and AChE inhibition by 6- and 2-fold, respectively. The ring-pruning of terminal phenyl group in **17** led to more flexible and basic **13**-**15**, whose fluorinated alkyl chains could mimic hydrophobic interactions performed by aromatic cycle. *Para*-substituted derivative **14** displayed a better B/A selectivity, as consequence of lower MAO A inhibition and higher MAO B potency than **13**. Restoring -CH_2OH at coumarin C4 produced the most active MAO B inhibitor (**15**, IC_{50} = 8.2 nM), endowed with outstanding selectivity (SI > 1250) along with strong and selective potency against AChE (IC_{50} = 550 nM). Upon inserting bioisosteric CF_2H-motif directly attached at the position 4 of the coumarin ring, a stronger HBD group was expected, as acidity was strictly dependent on substituent's EWG properties. Derivative **19**, strongly lipophilic, proved to be a well-balanced pan-inhibitor for relevant targets (MAO B, AChE and BChE; IC_{50} = 132, 561 and 430 nM, respectively), showing good B/A selectivity (SI > 73) and the lowest IC_{50} against BChE, at the submicromolar level.

Table 1. Inhibition data toward target enzymes for compounds **3-7**, **10-11**, **13-17**, **19-23**

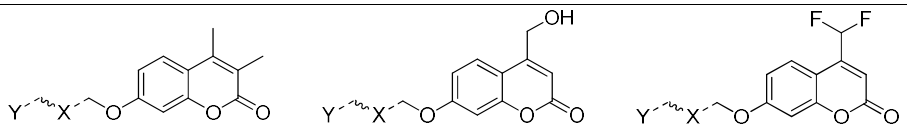

A B C

Cmpd	Gen. Struct.	Y	X	IC$_{50}$ (μM) or inhibition % at 10 μM[a]			
				*h*MAO-A[b]	*h*MAO-B[b]	*h*AChE[c]	*hs*BChE[d]
(±)-3	A	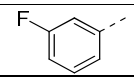	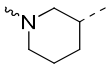	2.0±0.1	0.012±0.004	1.2±0.3	2.0±0.1
(±)-4	A	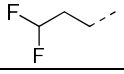		11±2	0.26±0.07	0.48±0.06	22±4%
5	A	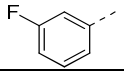	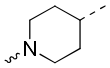	2.5±0.1	0.14±0.03	0.46±0.10	2.9±0.2
6	A	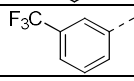		1.4±0.2	0.13±0.02	0.47±0.07	35±4%
7	A	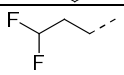		40±4%	0.53±0.11	1.2±0.1	8±2%
10	A	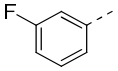	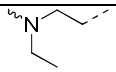	7.8±0.7	0.073±0.003	1.2±0.1	4.3±0.4
11	A		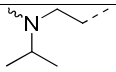	8.1±0.1	0.35±0.04	0.91±0.02	22±3%
13	A	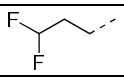	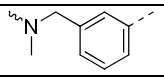	4.2±0.2	0.56±0.01	1.7±0.1	1.6±0.1
14	A	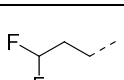	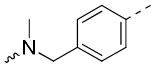	45±3%	0.16±0.02	1.5±0.2	4.1±0.7
15	B			34±2%	0.0082±0.0019	0.55±0.07	34±2%
16	B	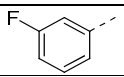		47±1%	0.010±0.003	0.33±0.04	1.1±0.1
17	B			15±2	0.010±0.002	0.12±0.01	1.1±0.3
19	C			17±3%	0.13±0.02	0.56±0.01	0.43±0.05
(±)-20	A	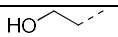	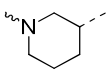	41±3%	1.5±0.1	1.1±0.1	26±3%
(±)-21	A			2.8±0.8	0.030±0.005	0.84±0.20	3.4±0.2
22	A	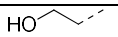	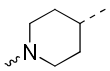	50±5%	0.48±0.05	0.89±0.12	30±3%
23	A			2.4±1.5	0.11±0.01	0.38±0.07	4.7±0.7
safinamide				20±3%	0.018±0.003	n.d.	n.d.
donepezil				n.d.	n.d.	0.023±0.003	2.1 ± 0.2

[a] Values are the mean of three independent experiments ± SEM. [b] Human recombinant MAOs on Supersomes. [c] Human AChE. [d] Horse serum BChE.

PAINS evaluation

Compounds under investigation were filtered by three in silico tools (ZINC15 pattern identifier,[44] PAINS remover,[45] FAF-Drugs4[46]) to identify potential Pan Assay Interference Compounds (PAINS)[47] linked to aggregating and/or undesirable structural scaffolds. Low-risk was associated to the fluorescence of coumarins that could produce interferences with the kynuramine-based spectrofluorimetric protocol readouts. A direct spectrophotometric method, measuring 4-hydroxyquinoline absorbance at 316 nm, although affected by lower sensitivity, was applied to the screening of some prototypes of *h*MAO B inhibitors (**5**, **11**, **15**, **16**). As reported in Table S1 (Supporting Information), IC_{50} values were close to those obtained in fluorescence thus excluding false positives among active compounds.

Physicochemical and early-ADME profiling

Table 2. Physicochemical properties of compounds **3**-**7**, **10**-**11**, **13**-**17**, **19**-**23**

Cmpd	*S* (μM)[a]	$LogD_{7.4}$[b]	$CHI_{pH7.4}$[c]
(±)-3	20±3	4.38	>100
(±)-4	349±5	2.67	83.4
5	11.0±0.5	3.43	>100
6	0.9±0.3[d]	5.05	>100
7	448±12	2.34	73.4
10	18±2	n.d.	>100
11	13±1	n.d.	>100
13	13±1	3.65	>100
14	13±1	3.78	>100
15	201±11	2.48	76.4
16	2.4±0.1[d]	4.29	>100
17	13±1	3.81	99.3
19	0.40±0.04[d]	4.80	>100
(±)-20	>500	1.15	48.8
(±)-21	33±2	3.65	>100
22	>500	0.86	47.3
23	57±4	3.40	99.7

[a] Kinetic solubility measured in PBS (pH 7.4) by UV/Vis spectrophotometric from triplicate experiments. Values are the mean of three independent experiments ± SEM. [b] 1-octanol/PBS (pH = 7.4) distribution coefficients determined through shake-flask method. Compound concentration was measured by HPLC-ES-MS/MS. [c] Chromatographic hydrophobicity index determined through a

fast gradient reversed-phase HPLC method. Values > 100 were not exactly indicated as they are outside the linearity range compared to retention time. [d] HPLC/MS analysis for sensitivity reasons.

At a first stage, physicochemical profiling addressed kinetic aqueous solubility determination at physiological pH (7.40) by means of UV or mass protocol. In addition, lipophilicity was assessed by determining $LogD_{7.4}$ (LC-MS) as well as chromatographic hydrophobicity index (CHI) in a fast-gradient RP-HPLC method, as indicated in Table 2.[48] The highest solubility values (> 500 μM) were returned by alcohols **(±)-20** and **22**, whereas both basicity attenuation and lipophilicity increase induced by benzyl group in **(±)-21** and **23** worsened solubility and partitioning parameters. As expected, the presence of F-arene moieties enhanced hydrophobicity indexes, thus compounds **(±)-3**, **5**, **10**, **11** displayed inadequate solubility (11 μM < Sol < 20 μM) for further development along with adverse distribution coefficients, even worsened by $-CF_3$ group (**6**). Bis-benzylamines **16-17** suffered from critical *S* values, affected by lower protonation degree at pH 7.4, as well as benzylamines **13-14**. Among fluorinated derivatives, more favourable physicochemical properties (solubility > 200 μM, CHI < 85, $LogD_{7.4}$ < 3) were restored by modulating pK_a in *N*-alkylpiperidines **(±)-4** and **7**, and by polar substituents at coumarin C4 (**15**) even though difluoromethyl groups determined a lipophilic penalty compared to alcohols (CHI < 50). Within the water-soluble series of achiral compounds, **7** and **15** exhibited more favourable physicochemical properties compared to **22**, whose extreme polarity, among other structural factors, contributed an outstanding solubility along with experimental $LogD_{7.4}$ value (0.84) quite lower than the calculated median (1.7) of marketed CNS drugs.[49] Indeed, the optimal extent (brain distribution) and rate (brain permeation through BBB) of central uptake depends on a well-balanced lipophilic/hydrophilic character. Moreover, the highly hydrophilic character for **22** could be associated to faster clearance.

After setting an arbitrary solubility threshold (20 μM), some derivatives were discriminated as poorly soluble and not progressed to permeation studies. Brain exposure to drugs depends on

several mechanisms (distribution, BBB permeation, efflux-pumps liability) that often underlie the attrition-rate for CNS-active agents. For orally administered drugs, adequate solubility and absorption from gastrointestinal (GI) tract is a pre-requisite for CNS penetration. Parallel artificial membrane permeability assay on hexadecane membrane (PAMPA-HDM) support was applied to assess in vitro the ability of compounds to permeate intestinal epithelial barrier by passive diffusion, thus endorsing oral bioavailability (Table 3). Apart from non-fluorinated **(±)-21** and **23**, all derivative enrolled in this assay were from moderate (**(±)-3**, **22**) to high permeant (**(±)-4**, **7**, **15**, **(±)-20**). Drug disposition within CNS is restricted to molecules able to permeate BBB and evade efflux machineries arranged at the apical surface of endothelial cells shielding brain from xenobiotics. PAMPA protocol on porcine brain lipid extracts (PAMPA-PBLE) models BBB permeation by transcellular passive diffusion, the main mechanism used for exogenous small molecules brain uptake. Again, BBB penetration for **(±)-3**, **(±)-21**, and **23** was hampered by retention whereas **(±)-4**, **7**, **15**, **(±)-20**, and **22** were predicted to passively permeate BBB and penetrate into CNS (Table 3), being **15** the best performer. Even though permeation occurs, brain accumulation can be still prevented by efflux systems such as P-gp, one of the most expressed pumps extruding drugs at BBB level. To address this issue, a cell-based model employing Caco-2 lines provided intestinal permeability estimation along with P-gp liability evaluation as these transporters are expressed at the apical surface (Table 3). For all investigated compounds, bidirectional transport studies returned optimal ER values (< 2) as the metric ruling out interactions with P-gp pump. Interestingly, fast permeability in both directions was scored by **15**, thus highlighting its well-balanced profile, whereas other samples from the studied subset were classified as moderately permeant across Caco-2 layer (0.2×10^{-5} cm/s < P_{app} < 2×10^{-5} cm/s).

Table 3. Permeation studies of selected compounds

cmpd	PAMPA-HDM[a]	PAMPA-BBB[b]		CACO-2 P_{app} ($\times 10^{-5}$ cm/s)[c]		
	LogP_a (cm/s)	P_e (10^{-6} cm/s)	classification	A → B	B → A	ER
(±)-3	-4.8±0.01	10.0±3.0	retention	--	--	--
(±)-4	-4.2±0.04	13.3±3.9	CNS +	--	--	--
7	-4.2±0.07	10.8±1.2	CNS +	1.7±0.6	1.6±0.1	1.0
15	-4.4±0.05	>14	CNS +	2.5±0.1	1.6±0.2	0.6
16	--	--	--	n.d.[d]	n.d.[d]	--
(±)-20	-4.4±0.01	7.2±0.8	CNS +	--	--	--
(±)-21	-5.0±0.02	--	retention	--	--	--
22	-4.7±0.04	6.0±0.1	CNS +	1.9±1.0	2.2±0.7	1.2
23	-5.0±0.16	--	retention	0.7±0.2	1.2±0.7	1.6

[a] Parallel Artificial Membrane Permeation Assay with a hexadecane artificial membrane. Values are the mean ± SD from duplicates. [b] Parallel Artificial Membrane Permeation Assay with Porcine Brain Lipid Extract (PBLE) dissolved in dodecane layer on a PVDF membrane support. Values are the mean ± SD from duplicates. [c] Apparent Permeability across Caco-2 cells monolayer. A → B: apical to basolateral direction. B → A: basolateral to apical direction. ER: efflux ratio = P_{app} B → A / P_{app} A → B. [d] not detectable, low recovery.

Metabolic stability is often a critical liability determining the success rate for medicinal chemistry programs, and transformations catalysed by microsomal enzymes represent a major route for disposing of bioactive compounds (and their metabolites) through hepatic clearance thus affecting drug's bioavailability and half-life. Fluorine and F-containing motifs have been largely exploited as structural tools to encumber the activity of metabolizing enzymes, thanks to the niche of physicochemical properties (electronegativity, size, dipole moment and bond-dissociation energy). In all compounds recruited for stability studies in mouse liver microsomes (MLM, see Table 4), the presence of EWG fluorinated groups on aromatic rings was unable to restore appreciable half-lives with respect to unsubstituted analogues (**(±)-21** vs **(±)-3**, **5**-**6** vs **23**), ruling out hot spots in this region reliably. As could be expected, more lipophilic -CF_2H bioisostere produced higher clearance in mouse microsomal preparations, making compounds **7** and **(±)-4** much more labile than alcohols **22** and **(±)-20**, respectively. Interestingly, compounds bearing a -CH_2OH group at coumarin C4 did not suffer from metabolic liabilities, even tempered by *meta*-F substitution (**16**-**17**; $t_{1/2}$ = 31.7 and 36.9 minutes, respectively). Given the potent in vitro inhibitory activities along with favourable

preliminary physicochemical and permeation features displayed by **7**, **15** and **22**, these compounds were also tested in human liver microsomes (HLM). Even more surprisingly, fluorinated **7** showed greatly enhanced half-life when tested in human liver microsomes, though confirming its higher instability than parent **22** (> 120 min). The high metabolic stability of dual hit **15** in MLM ($t_{1/2}$ = 25 minutes, CL_{int} = 55.6 μL/min/mg protein) endorsed its remarkable drug-like profile, exhibiting also lower clearance in HLM ($t_{1/2}$ = 34.9 minutes, CL_{int} = 39.8 μL/min/mg protein).

Table 4. Microsomal stability, clearance and inhibition of human CYP3A4

cmpd	Microsomal stability[a] $t_{1/2}$ (min)		CL_{int}[b]		CYP3A4 (IC_{50}, μM)[c]
	mouse	human	mouse	human	
(±)-3	6.6±0.1		209.8 ± 0.1		
(±)-4	17.8±0.5		78.1±4.2		>10
5	6.2±0.2		224.9±7.7		
6	9.5±0.3		146.4±4.3		
7	11.9±1.2	98.9±4.1	116.3±11.5	14.1±0.6	0.8±0.1
10	5.3±0.8		260.4± 36.2		
13	4.8±0.9		288.6±9.4		0.6±0.1
15	25.0±2.8	34.9±0.9	55.6±6.2	39.8±1.0	10±2.3
16	36.9±2.2		37.7±2.3		3.5±0.6
17	31.7±0.1		43.9±0.1		7±0.9
19	9.8±0.1		141.9±0.9		
(±)-20	92.4±12.6		15.1±3.1		
(±)-21	5.3±0.1		264.7±4.5		
22	47.2±3.2	> 120	29.5±1.9	<11.5	>10
23	6.7±0.2		206.3±6.7		
ketoconazole					0.025±0.003

[a] Values are the mean ± SD from duplicates. [b] Intrinsic clearance expressed in μL/min/mg protein. Values are the mean ± SD from duplicates. [c] Recombinant CYP450 proteins used in a fluorescent homogenous assay. Values are the mean ± SD from triplicates.

Very often, adverse effects coming from co-administered drugs are the consequence of inhibited metabolic machineries involving cytochromes within hepatocytes. Being one the five major isoforms, CYP3A4 was used to probe the chance of drug-drug interactions related to metabolism blockade. At a first glance, no clear correlation between inhibition of CYP3A4 and structural motifs

(or related physicochemical parameters) could be envisaged for the subset displayed in Table 4. For instance, both derivatives **15** and **22** behaved as weak CYP3A4 inhibitors, suggesting that their slow metabolic clearance is unrelated to self-inhibiting metabolic processes, whereas a close congener of **15** (compound **13**) was found as a potent inhibitor. Interestingly, strong CYP3A4 inhibition (IC_{50} = 0.8 μM) might account, at least in part, for the much greater metabolic stability displayed by compound **7** in HLM than in MLM.

Both tissue specific and non-specific cytotoxicity was studied by measuring the effect on cell viability (ATP detection assay with respect to control, in the absence of compounds) upon co-incubating selected samples with human neuroblastoma (SH-SY5Y) and hepatocarcinoma (HepG2) cell lines as prototypes for neuronal and hepatic cells, respectively. As displayed in Figure 2, most compounds were devoid of cytotoxic effects also at the highest concentrations applied (100 μM). Both alcohols **(±)-20** and **22** did not impair cell viability in both cultures, whereas, among fluorinated derivatives, **15** demonstrated the safest profile showing only negligible alteration of viable SH-SY5Y cells when assayed at 100 μM along with non-toxic activity at all against HepG2 lines. The only exception was represented by coumarin **16**, whose moderate cellular damage returned IC_{50} = 40 μM in both lines.

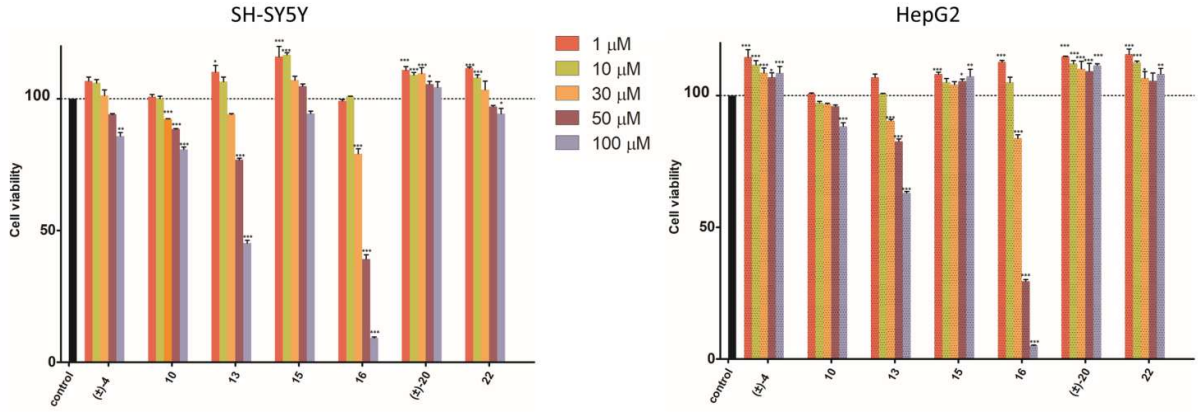

Figure 2. Viability of SH-SY5Y and HepG2 cells in the presence of compounds **10**, **13**, **15-16**, **(±)-20**, **22** at different concentrations measured through CellTiter-Glo Luminescent Cell Viability Assay and showed as means ± SD of three independent experiments, each performed in triplicates and referred to untreated control cells (control, 100% values, in the absence of compound).

Statistical significance was calculated using a two-way analysis of variance (ANOVA) followed by the Bonferroni post-hoc tests (GraphPad Prism version 5); * $p < 0.05$, ** $p < 0.01$, *** $p < 0.001$.

Investigation of hit compound 15

In light of preliminary physicochemical and early-ADME data profiling, achiral CF_2H-bearing coumarin **15** emerged as a hit compound endowed with potent in vitro dual AChE-MAO B inhibition along with the most promising metabolic, physicochemical, safety, and CNS-distribution features.

Inhibition kinetics

The kinetics of inhibition of compound **15** was studied toward both target enzymes (*h*MAO B and *h*AChE). As inferred from Figure 3A, coumarin **15** behaved as a competitive *h*MAO B inhibitor with K_i = 13 ± 2 nM. In order to shed light on the mechanism of action, the residual enzymatic activity was studied in a time-course experiment, with and without pre-incubating the enzyme in the presence of the inhibitors (Figure S2). Derivative **15** (10 nM) showed the same time-course evolution in both experiments, unrelated to pre-incubation. A close behaviour was performed by safinamide (10 nM), a well-known reversible MAO B inhibitor. On the contrary, pargyline (100 nM) fully blocked enzymatic activity upon 1 h pre-incubation as for covalent irreversible propargylamine inhibitors. Regarding AChE inhibition kinetics, Lineweaver-Burk plots in Figure 3B was typical of a mixed-mode inhibition (K_i = 2.0 ± 0.3 μM) and suggested partial PAS occupancy for **15** as expected for dual-binding site AChE inhibitors.

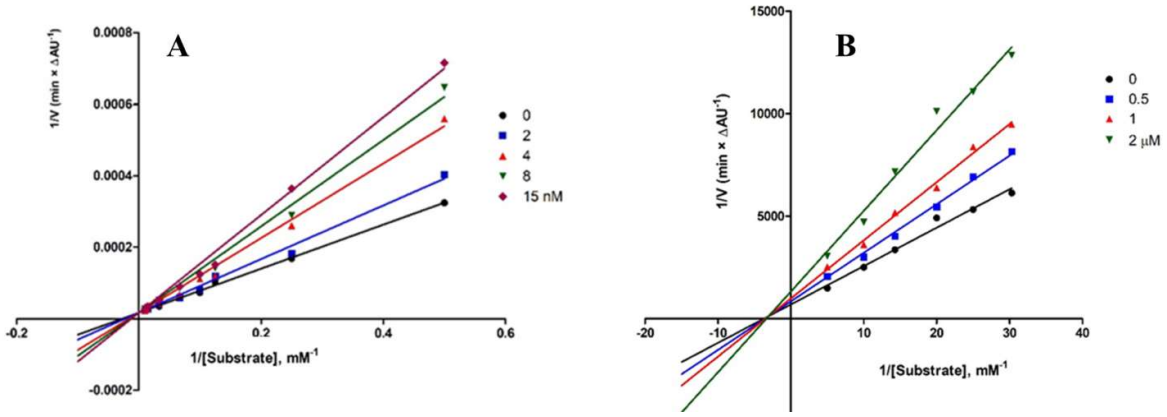

Figure 3. Lineweaver−Burk plots of inhibition kinetics for compound **15** towards *h*MAO B (A) and *h*AChE (B). Reciprocals of enzyme activity vs reciprocals of substrates' concentration in the presence of different inhibitor's concentrations (0−15 nM for *h*MAO B, 0−2 μM for *h*AChE; reported in inserts).

Neuroprotection studies

After ensuring the absence of inherent cytotoxicity induced by derivative **15** on neuroblastoma line at the concentrations under study, MTT assay was applied to determine the percentage of viable cells co-incubated with **15** and two different insults, namely hydrogen peroxide (H_2O_2, 50 μM, 4A) and *N*-methyl-D-aspartate (NMDA, 250 and 500 μM, 4B). Even if lower than standard quercetin (used as positive control), the neurorescue ability of **15** against pro-oxidant H_2O_2 (co-incubated at 50 μM) was statistically significant at 1 and 5 μM. Moreover, as shown in Figure 4B, this compound greatly increased the number of viable cells insulted by NMDA, completely neutralizing the cytotoxic effect of the insult (250-500 μM) also when co-incubated at nanomolar concentration. Interestingly, the protective activity was comparable to that of donepezil at the same concentrations, used as standard anti-Alzheimer drug.

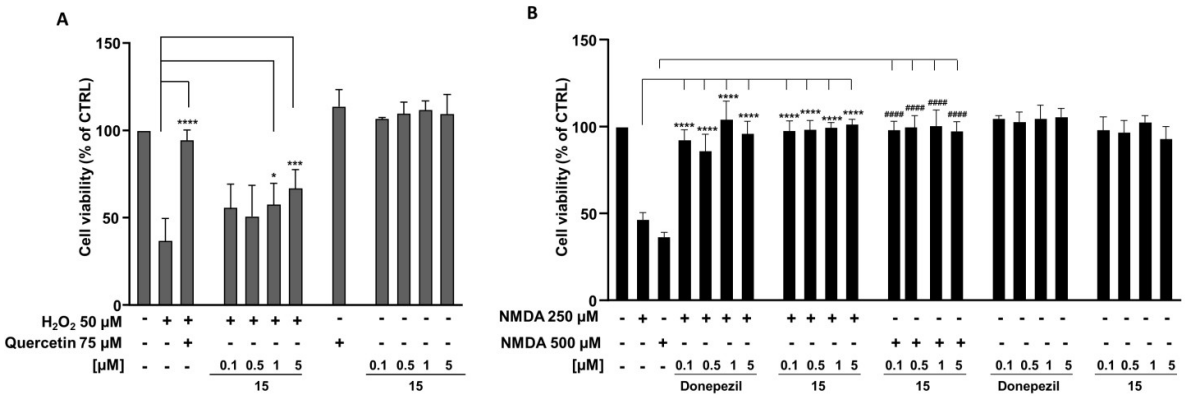

Figure 4. Effect of compound **15** at 0.1-5 µM concentrations on viable SH-SY5Y cells in the absence and presence of toxic insults (H_2O_2, 50 µM, A; NMDA, 250 and 500 µM, B) after co-incubation for 24 h. Viability was measured through MTT test and is presented as means ± SD of three independent experiments, each performed in triplicates and referred to untreated control cells (CTRL, 100% values). Quercetin (75 µM) and donepezil (0.1-5 µM) were used as positive controls, as standard antioxidant and anti-AD reference drug, respectively. Statistical analysis was done by applying one-way ANOVA followed by multiple comparison tests (Dunnett's test). Levels of significance: **** $p < 0.0001$, *** $p < 0.001$, *$p < 0.05$, ####$p < 0.0001$.

Albumin binding

The evaluation of Human Serum Albumin (HSA) binding for **15** and non-fluorinated congener **22**, for comparative purposes, was performed by Surface Plasmon Resonance (SPR) using warfarin as a reference compound.[50,51] Being the most abundant plasma protein, HSA binding can deeply influence drug bioavailability and then plays a central role in the ADME profile of xenobiotics. Indeed, the estimation of HSA affinity can be assessed in the earlier steps of hit discovery. The association (k_{on}) and dissociation (k_{off}) rate constants resulted too fast to be calculated with good approximation, and both **15** and **22** can be considered as fast and reversible HSA binders. They further resulted as moderate HSA binders, showing K_D = 31.7 and 11.3 µM for **22** and **15** (Figure S3), respectively, higher than reference warfarin (K_D = 5.5 µM), considered a strong HSA binder.[52] Interestingly, derivative **15** (K_D = 11.3 µM) bearing a difluoromethyl group, as more lipophilic and weaker hydrogen bonding (HB) donor bioisostere for hydroxyl, showed HSA affinity three fold higher than alcohol **22** (K_D = 31.7 µM). However, at physiological HSA plasma concentration

(about 680 μM), compound **15** (at 10 μM concentration) was predicted to achieve 20-40% albumin binding, thus returning good bioavailability.

Molecular docking simulations

Molecular docking simulations were carried out to shed light on binding poses played by **15** within target enzymes. Human AChE and MAO B coded as 4EY7 and 2V5Z, respectively, were retrieved from Protein Data Bank (PDB). Regarding hAChE (Figure **5A**), the coumarin core of **15** packed against PAS, where it was anchored through a face-to-face arene-arene interaction occurring with Trp286, and a hydrogen bonding network involving the lateral CH_2OH chain. The binding was further stabilized by additional π-π stacking between the aromatic linker and the side chain of Tyr341 lining the mid-gorge in an open conformation. Bridge flexibility allowed the basic chain to fit CAS, by means of the positively charged amine interacting with both the indole ring of Trp86 and Tyr337 side chain, and to orient the fluorinated chain toward the oxyanionic hole. The burying of the inhibitor within the active site, fully occupied from PAS to CAS, was in agreement with the mixed-mode kinetics returned by **15**. The binding pose within MAO B is illustrated in Figure **5B**, showing the inhibitor fully buried within the enzymatic cavity lined by aromatic residues. The coumarin is accommodated close to FAD stacking in front of Tyr398 (π-π interaction) and Tyr188 through a bidentate HB with phenolic OH and Cys172 carbonyl. The flipping of the xylyl linker permitted a molecular folding that escaped steric clashes with gating Ile199, upon interacting with Tyr326, whereas the aliphatic chain pointed at outer regions.

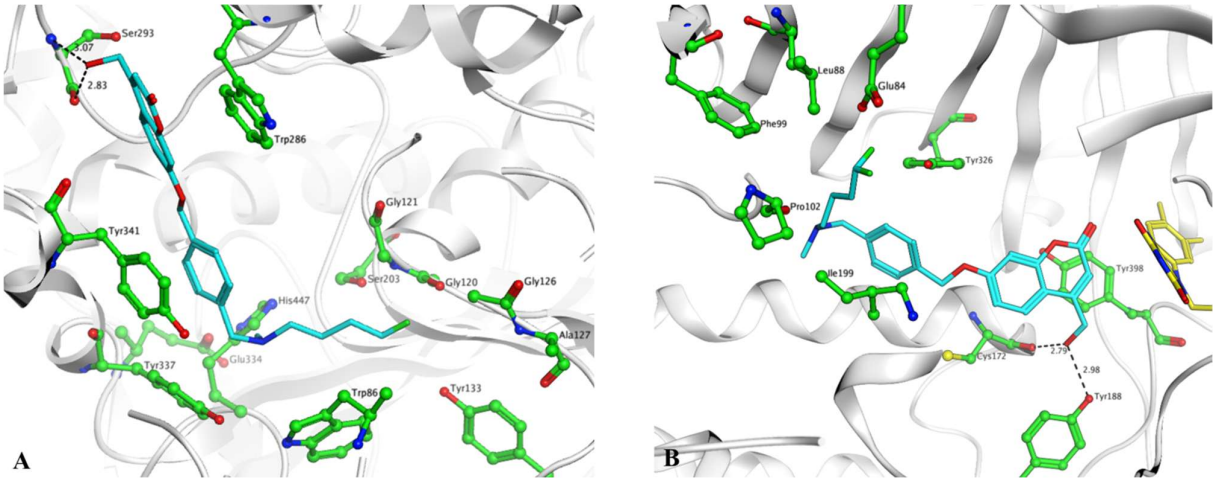

Figure 5. Top-scored binding poses of compound **15** docked within *h*AChE (A, PDB 4EY7, -10.79 kcal/mol) and *h*MAO B (B, PDB 2V5Z, -10.88 kcal/mol). Ligand is rendered as sticks, relevant amino acid residues are rendered as ball-and-sticks, while protein is represented as a cartoon. Colours are in according to the atom code, C atoms in cyan and green for ligand and amino acid, respectively. Residues forming AChE catalytic triad (Glu334-His447-Ser203) are rendered as semi-transparent ball-and-sticks (6A). Carbon atoms of FAD coenzyme in human MAO B are coloured in yellow and depicted as sticks (6B). Dotted lines represent HB.

Conclusions

As a part of our ongoing research aimed at discovering neuroprotective dual AChE-MAO B inhibitors, here we exploited H/F and CH_2OH/CF_2H bioisosteric replacement to develop novel coumarin-based multitarget inhibitors. Given that the introduction of fluorine and fluorinated motifs could strongly modulate relevant properties (binding affinity, basicity, bioavailability, metabolic stability) for medicinal chemistry research, in vitro screening toward target enzymes was followed by drug-likeness evaluation enrolling the most promising hits, hierarchically advanced to each step of early-ADME profiling that addressed solubility, CNS-penetration, cytotoxicity, bioavailability predictors (metabolic stability, albumin binding, Caco-2 permeation). Fluorinated motifs were well-tolerated by target enzymes even if no specific direct binding interactions with F was retrieved in docking analysis. As expected, fluorine deeply influenced physicochemical properties. On the other side, cytotoxicity, CNS-distribution, and microsomal stability were affected to a lesser extent. Taking advantage of an optimal hydrophilic/lipophilic balance allowed by CF_2H motif as a weak and lipophilic HB donor, compound **15** displayed outstanding in vitro targets' inhibition (IC_{50} = 550

nM and 8.2 nM for AChE and MAO B, respectively) along with a promising drug-like character. This coumarin showed high solubility and brain-permeant features. The oral bioavailability of **15** was strongly supported by poor drug-drug interaction liability, good metabolic stability, moderate binding to plasma albumin, fast transport across Caco-2 lacking P-gp efflux. In SH-SY5Y and HepG2 cell lines, **15** produced negligible cytotoxic effects. Moreover, it was able to reduce the neuronal damage produced by H_2O_2 and to fully switching off the toxicity of high doses NMDA in neuroblastoma culture. In light of these preliminary data, this compound will deserve further evaluation in in-vivo pharmacokinetic mouse studies and then in AD animal models to validate its neuroprotective activity, after scaling-up and optimizing the synthesis with the aim of reducing the impact of hazardous DAST.

Experimental part

Chemistry.

Starting materials, reagents, and analytical grade solvents were purchased from Sigma-Aldrich, Alfa-Aesar or Fluorochem (Europe). The purity of all the intermediates, checked by RP-HPLC, was always better than 95%. RPLC analyses were performed on an Analytic Agilent 1260 Infinity multidetector system equipped with automatic sampler and a 1200 series UV-diode array detector by using a Kinetex 2.6 mm C18 column (150 mm × 2.1 mm I. D.). UV detection was measured at 230, 254, 280 and 320 nm. Each tested compound was analysed by isocratic elution with two different mobile phase systems: in system 1, compounds were eluted using a 70/30 methanol/ammonium formate buffer (10 mM, pH 4.5) mixture at a flow rate of 0.2 or 0.5 mL/min; in system 2, compounds were eluted using a 65/35 acetonitrile/ammonium formate buffer (10 mM, pH 4.5) mixture at a flow rate of 0.2 or 0.5 mL/min. All the newly prepared and tested compounds showed purity higher than 95% (elemental analysis). Elemental analyses were performed on the EuroEA 3000 analyzer only on the final compounds tested as MAOs and ChEs inhibitors. The measured values for C, H, and N agreed to within ± 0.40% of the theoretical values. Microwave reactions were performed in a Milestone MicroSynth apparatus, setting temperature and hold times, fixing maximum irradiation power to 500 W and heating ramp times to 2 minutes. Column chromatography was performed using Merck silica gel 60 (0.063-0.200 mm, 70-230 mesh). Flash chromatographic separations were performed on Biotage SP1 purification system using flash

cartridges prepacked with KP-Sil 32-63 μm, 60 Å silica. All reactions were routinely checked by TLC using Merck Kieselgel 60 F_{254} aluminum plates and visualized by UV light. Regarding the reaction requiring the use of dry solvents, the glassware was flame-dried and then cooled under a stream of dry argon before the use. Nuclear magnetic resonance spectra were recorded on a Varian Mercury 300 instrument (at 300 MHz) or on a Agilent Technologies 500 apparatus (at 500 MHz) at ambient temperature in the specified deuterated solvent. Chemical shifts (δ) are quoted in parts per million (ppm) and are referenced to the residual solvent peak. The coupling constants *J* are given in Hertz (Hz). The following abbreviations were used: s (singlet), d (doublet), dd (doublet of doublet), ddd (doublet of doublet of doublet), t (triplet), q (quadruplet), qn (quintuplet), m (multiplet), br s (broad signal); signals due to OH and NH protons were located by deuterium exchange with D_2O. HRMS experiments were performed with a dual electrospray interface (ESI) and a quadrupole time-of-flight mass spectrometer (Q-TOF, Agilent 6530 Series Accurate-Mass Quadrupole Time-of-Flight LC/MS, Agilent Technologies Italia S.p.A., Cernusco sul Naviglio, Italy). Full-scan mass spectra were recorded in the mass/charge (m/z) range 50-3000 Da. Melting points for solid final compounds were determined by the capillary method on a Stuart Scientific SMP3 electrothermal apparatus and are uncorrected. The following compounds have been already described in the literature: 4-hydroxybutyl benzoate **1a**,[53] 3,4-dimethyl-7-(piperidin-3-ylmethoxy)-2*H*-chromen-2-one **2a**,[31] 3,4-dimethyl-7-(piperidin-4-ylmethoxy)-2*H*-chromen-2-one **2b**,[31] (3-fluorobenzyl)piperidin-3-yl]methoxy}-3,4-dimethyl-2*H*-chromen-2-one **(±)-3**,[54] 7-(3-bromopropoxy)-3,4-dimethyl-2*H*-chromen-2-one **9a**,[55] 7-{[4-(bromomethyl)benzyl]oxy}-4-(hydroxymethyl)-2*H*-chromen-2-one **9b**,[32] 7-((3-(chloromethyl)benzyl)oxy)-3,4-dimethyl-2*H*-chromen-2-one **9c**,[18] 7-((4-(bromomethyl)benzyl)oxy)-3,4-dimethyl-2*H*-chromen-2-one **9d**,[18] 7-{[1-7-[(4-{[benzyl(methyl)amino]methyl}benzyl)oxy]-4-(hydroxymethyl)-2*H*-chromen-2-one **17**,[32] 7-{[1-(3-hydroxypropyl)piperidin-3-yl]methoxy}-3,4-dimethyl-2*H*-chromen-2-one **(±)-20**,[18] 7-[(1-benzylpiperidin-3-yl)methoxy]-3,4-dimethyl-2*H*-chromen-2-one **(±)-21**,[31] 7-{[1-(3-hydroxypropyl)piperidin-4-yl]methoxy}-3,4-dimethyl-2*H*-chromen-2-one **22**,[18] 7-[(1-benzylpiperidin-4-yl)methoxy]-3,4-dimethyl-2*H*-chromen-2-one **23**.[31]

4-Oxobutyl benzoate 1b. A solution of **1a**[53] (23 mmol, 4.5 g) in anhydrous CH_2Cl_2 (15 mL) was dropped into a stirred suspension of pyridinium chlorochromate (PCC) (35 mmol, 7.4 g) and celite (8 g) in CH_2Cl_2 (50 mL) in a two-necked round-bottom flask. The resulting dark-brown mixture was kept at room temperature for 1.5 h and then diluted with anhydrous Et_2O (180 mL) and filtered through a celite pad. The solvents were evaporated under reduced pressure and the crude residue was purified by flash chromatography (gradient eluent: ethyl acetate in *n*-hexane, 0% → 20%) to give the pure aldehyde **1b** as a colorless oil. Yield: 82%. ^{1}H NMR (500 MHz, $CDCl_3$) δ: 9.84 (t, *J* =

1.1 Hz, 1H), 8.02 (ddd, *J* = 8.5, 3.4, 1.4 Hz, 2H), 7.63 – 7.52 (m, 1H), 7.48 – 7.36 (m, 2H), 4.36 (t, *J* = 6.8 Hz, 2H), 2.64 (t, *J* = 6.8 Hz, 2H), 2.12 (qn, *J* = 6.8 Hz, 2H).

4,4-Difluorobutyl benzoate 1c. To a stirred solution of **1b** (11 mmol, 2.1 g) in dry CH_2Cl_2 (20 mL), (diethylamino)sulfur trifluoride (DAST; 20 mmol, 2.6 mL) was added dropwise at 0 °C *via* syringe under N_2 atmosphere. After 10 minutes, the reaction mixture was allowed to warm to room temperature and stirred for additional 50 minutes. The reaction mixture was then cooled to 0 °C and carefully quenched with 20 mL saturated $NaHCO_3$. The mixture was then extracted with CH_2Cl_2 (3 x 40 mL). The collected organic layers were dried over anhydrous Na_2SO_4 and concentrated under rotary evaporation. The crude residue was purified by column chromatography (eluent: ethyl acetate in *n*-hexane, 0.5%). Yield: 40%. ^{1}H NMR (300 MHz, $CDCl_3$) δ: 8.09 – 7.98 (m, 2H), 7.61 – 7.51 (m, 1H), 7.49 – 7.39 (m, 2H), 5.90 (tt, *J* = 56.5, 4.0 Hz, 1H), 4.37 (t, *J* = 6.0 Hz, 2H), 2.20 – 1.83 (m, 4H).

4,4-Difluorobutyl 4-nitrobenzenesulfonate 1d. By applying slight modifications to a reported procedure,[39] sodium methoxide powder (4.8 mmol, 0.26 g) was added in one portion to a stirred solution of **1c** (3.2 mmol, 0.68 g) in MeOH **(**10 mL**)** cooled to 0 °C. After 1.5 h at room temperature, TFA (4.8 mmol, 0.37 mL) was added while cooling at 0 °C and the clear mixture was stirred for 30 minutes at room temperature. Methanol was then removed under rotary evaporation and the residue partitioned between Et_2O (20 mL) and brine (40 mL). The aqueous layer was extracted with Et_2O (3 x 20 mL), then the organic phases were collected and concentrated to dryness. The crude product was dissolved in dry CH_2Cl_2 (20 mL) followed by the addition of Et_3N (4.8 mmol, 0.66 mL), 4-nitrobenzenesulfonyl chloride (3.8 mmol, 0.84 g) and 4-(dimethylamino)pyridine (DMAP; 0.32 mmol, 0.040 g). The reaction mixture was stirred at room temperature for 1.5 h, then quenched with saturated NH_4Cl (40 mL) and extracted with ethyl acetate (3 x 30 mL). The collected organic layers were dried over Na_2SO_4 and concentrated under reduced pressure. The resulting crude was purified by column chromatography (gradient eluent: ethyl acetate in *n*-hexane, 0% → 20%) to afford difluoride **1d** as a yellow oil. Yield: 38%. ^{1}H NMR (500 MHz, $CDCl_3$) δ: 8.44 – 8.39 (m, 2H), 8.14 – 8.07 (m, 2H), 5.84 (tt, *J* = 56.3, 3.6 Hz, 1H), 4.21 (t, *J* = 5.9 Hz, 1H), 2.01 – 1.82 (m, 4H).

General procedures for *N*-alkylation reactions.

Method A. Piperidine intermediate **2b**[31] (0.34 mmol, 0.10 g) was suspended in acetonitrile (1.5 mL) before adding anhydrous K_2CO_3 (0.68 mmol, 0.096 g) and the suitable benzyl bromide (0.34 mmol). The reaction was refluxed for 5 h and the solvent was evaporated under reduced pressure.

The resulting crude was suspended in CH_2Cl_2 and the inorganic solid residue was filtered off after thoroughly washing. The solvent was removed under rotary evaporation and the desired products were isolated as described below.

Method B. To a solution of appropriate amine (30 mmol) in THF (6 mL) aliquots (0.4 mL) of 3-fluorobenzylbromide (1.5-3.0 mmol) previously dissolved in THF (3.0 mL) were added every 45 minutes' intervals (after TLC monitoring to check bromide consumption). The excess amine was evaporated, then the reaction mixture was diluted with brine (20 mL) and extracted with CH_2Cl_2 (3 x 10 mL). The collected organic layers were dried over anhydrous Na_2SO_4, concentrated under rotary evaporation and purified by flash chromatography (gradient: methanol in dichloromethane, 0% → 10%).

Method C. Intermediate **9a**[55] (0.20 mmol, 0.062 g) was solubilized in acetonitrile (4 mL). K_2CO_3 (0.40 mmol, 0.055 g), appropriate amine (0.40 mmol) and a catalytic amount of KI were added. The reaction mixture was refluxed under magnetic stirring for 10 h. After cooling at room temperature, the mixture was concentrated to dryness and the residue was suspended with CH_2Cl_2. The inorganic solid was filtered off and washed with CH_2Cl_2. The solvent was removed under rotatory evaporation and the resulting crude was purified through flash chromatography (gradient: methanol in dichloromethane, 0% → 5%).

Method D. Derivatives **9b,**[32] **9c-d**[18] (0.50 mmol) were dissolved in THF (1.6 mL). Aliquots (0.2 mL) of this solution were added at 45 minutes' intervals under N_2 atmosphere to a round bottom flask containing commercially available 2.0 M CH_3NH_2 solution in THF (5.0 mL). Once additions were completed, the reaction mixture was left at room temperature under magnetic stirring overnight. The excess methylamine and THF was evaporated to dryness. The resulting crude was purified as described below.

Method E. The appropriate intermediate **2a-b**[31] or **12a-c** (0.24 mmol) was dissolved in acetonitrile (1 mL) followed by the addition of K_2CO_3 (0.24 mmol, 0.033 g). Intermediate **1d** (0.22 mmol, 0.065 g) was then added to this mixture. The vessel was sealed and the resulting reaction mixture was left under magnetic stirring at 80 °C for 18 hours. After cooling to room temperature, the reaction was concentrated to dryness. The solid residue was dissolved in $CHCl_3$ and the inorganic residue was filtered off. The solution was concentrated under reduced pressure and the resulting crude was purified as described below.

7-{[1-(4,4-Difluorobutyl)piperidin-3-yl]methoxy}-3,4-dimethyl-2*H*-chromen-2-one (±)-4. Method E: prepared from **2a** (0.24 mmol, 0.069 g). Purification procedure: column chromatography

(gradient eluent: methanol in CH_2Cl_2, 0% → 2%). Yield: 51%; white solid; mp: 74-76 °C. ^{1}H NMR (300 MHz, $CDCl_3$) δ: 7.48 (d, *J* = 8.8 Hz, 1H), 6.84 (dd, *J* = 8.8, 2.4 Hz, 1H), 6.78 (d, *J* = 2.4 Hz, 1H), 5.86 (tt, *J* = 56.7, 4.3 Hz, 1H), 3.93 – 3.82 (m, 2H), 3.06 – 2.93 (m, 1H), 2.90 – 2.76 (m, 1H), 2.46 – 2.38 (m, 2H), 2.37 (s, 3H), 2.18 (s, 3H), 2.09 – 1.88 (m, 2H), 1.87 – 1.76 (m, 2H), 1.76 – 1.67 (m, 3H), 1.67 – 1.52 (m, 4H). ^{13}C NMR (126 MHz, $CDCl_3$) δ: 162.48 (s), 160.97 (s), 153.52 (s), 146.25 (s), 125.18 (s), 118.85 (s), 117.30 (t, *J* = 238.7 Hz), 114.09 (s), 112.43 (s), 101.03 (s), 71.32 (s), 58.02 (s), 57.01 (s), 54.04 (s), 36.07 (s), 32.13 (t, *J* = 21.0 Hz), 27.24 (s), 24.67 (s), 19.51 (t, *J* = 5.3 Hz), 15.09 (s), 13.15 (s). Anal. ($C_{21}H_{27}F_2NO_3$) calcd. % C, 66.47; H, 7.17; N, 3.69; found % C, 66.90; H, 6.91; N, 3.81. HRMS (Q-TOF) Calcd for ($C_{21}H_{27}F_2NO_3$): $[M+H]^+$ m/z: 380.2032, found 380.2046; $[M+Na]^+$ m/z: 402.1851, found 402.1864.

7-{[1-(3-Fluorobenzyl)piperidin-4-yl]methoxy}-3,4-dimethyl-2*H*-chromen-2-one 5. Method A: prepared from 3-fluorobenzyl bromide (0.34 mmol, 0.042 mL). Purification procedure: column chromatography (eluent: ethyl acetate in CH_2Cl_2, 50%). Yield: 64%; white solid; mp: 123-126 °C. ^{1}H NMR (300 MHz, $CDCl_3$) δ: 7.48 (d, *J* = 8.8 Hz, 1H), 7.32 – 7.21 (m, 1H), 7.13 – 7.02 (m, 2H), 6.99 – 6.90 (m, 1H), 6.83 (dd, *J* = 8.8, 2.5 Hz, 1H), 6.78 (d, *J* = 2.5 Hz, 1H), 3.85 (d, *J* = 5.8 Hz, 2H), 3.51 (s, 2H), 2.99 – 2.86 (m, 2H), 2.37 (s, 3H), 2.18 (s, 3H), 2.09 – 1.93 (m, 2H), 1.88 – 1.73 (m, 3H), 1.53 – 1.35 (m, 2H). ^{13}C NMR (126 MHz, DMSO-*d*$_6$) δ: 158.16 (d, *J* = 245.3 Hz), 157.67 (s), 156.27 (s), 148.78 (s), 141.45 (s), 136.57 (d, *J* = 5.0 Hz), 124.79 (d, *J* = 8.2 Hz), 120.42 (s), 119.72 (d, *J* = 2.7 Hz), 114.08 (s), 110.93 (d, *J* = 21.3 Hz), 109.32 (s), 109.04 (d, *J* = 21.2 Hz), 107.58 (s), 96.35 (s), 68.24 (s), 58.00 (d, *J* = 1.4 Hz), 48.53 (s), 30.94 (s), 24.20 (s), 10.33 (s), 8.43 (s). Anal. ($C_{24}H_{26}FNO_3$) calcd. % C, 72.89; H, 6.63; N, 3.54; found % C, 73.12; H, 6.50; N, 3.59. HRMS (Q-TOF) Calcd for ($C_{24}H_{26}FNO_3$): $[M+H]^+$ m/z: 396.1969, found 396.1979; $[M+Na]^+$ m/z: 418.1789, found 418.1807.

3,4-Dimethyl-7-({1-[3-(trifluoromethyl)benzyl]piperidin-4-yl}methoxy)-2*H*-chromen-2-one 6. Method A: prepared from 3-(trifluoromethyl)benzyl bromide (0.34 mmol, 0.052 mL). Purification procedure: flash chromatography (gradient eluent: ethyl acetate in dichloromethane, 0% → 30%). Yield: 80%; white solid; mp: 113-115 °C. ^{1}H NMR (500 MHz, DMSO-*d*$_6$) δ: 7.66 (d, *J* = 9.6 Hz, 1H), 7.63 – 7.57 (m, 3H), 7.57 – 7.52 (m, 1H), 6.95 – 6.88 (m, 2H), 3.92 (d, *J* = 5.9 Hz, 2H), 3.54 (s, 2H), 2.88 – 2.74 (m, 2H), 2.34 (s, 3H), 2.05 (s, 3H), 2.02 – 1.90 (m, 2H), 1.79 – 1.67 (m, 3H), 1.38 – 1.22 (m, 2H). ^{13}C NMR (126 MHz, DMSO-*d*$_6$) δ: 157.67 (s), 156.24 (s), 148.78 (s), 141.44 (s), 134.84 (s), 127.58 (s), 125.79 (q, *J* = 31.9 Hz), 123.89 (s), 120.85 (s), 120.54 (q, *J* = 272.2 Hz), 120.43 (s), 119.12 (s), 114.10 (s), 109.35 (s), 107.57 (s), 96.36 (s), 68.17 (s), 57.96 (s), 48.52 (s), 30.89 (s), 24.15 (s), 10.29 (s), 8.38 (s). Anal. ($C_{25}H_{26}F_3NO_3$) calcd. % C, 67.40; H, 5.88; N, 3.14;

found % C, 67.84; H, 6.01; N, 3.03. HRMS (Q-TOF) Calcd for ($C_{25}H_{26}F_3NO_3$): $[M+H]^+$ m/z: 446.1938, found 446.1945; $[M+Na]^+$ m/z: 468.1757, found 468.1770.

7-{[1-(4,4-Difluorobutyl)piperidin-4-yl]methoxy}-3,4-dimethyl-2*H*-chromen-2-one 7. Method E: prepared from **2b** (0.24 mmol, 0.069 g). Purification procedure: column chromatography (gradient eluent: methanol in dichloromethane, 0% → 2%). Yield: 46%; pale-yellow solid; mp: 102-104 °C. ^{1}H NMR (500 MHz, $CDCl_3$) δ: 7.48 (d, *J* = 8.9 Hz, 1H), 6.83 (dd, *J* = 8.9, 2.5 Hz, 1H), 6.78 (d, *J* = 2.5 Hz, 1H), 5.86 (tt, *J* = 57.0, 4.4 Hz, 1H), 3.85 (d, *J* = 5.9 Hz, 2H), 2.96 (d, *J* = 11.2 Hz, 2H), 2.39 (t, *J* = 7.4 Hz, 2H), 2.36 (s, 3H), 2.18 (s, 3H), 1.98 (t, *J* = 11.3 Hz, 2H), 1.92 – 1.78 (m, 5H), 1.67 (qn, *J* = 7.4 Hz, 2H), 1.51 – 1.36 (m, 2H). ^{13}C NMR (126 MHz, $CDCl_3$) δ: 162.40 (s), 160.91 (s), 153.52 (s), 146.17 (s), 125.21 (s), 118.90 (s), 117.12 (t, *J* = 237.5 Hz), 114.15 (s), 112.25 (s), 101.15 (s), 72.75 (s), 57.76 (s), 53.19 (s), 35.60 (s), 32.07 (t, *J* = 21.4 Hz), 28.65 (s), 19.32 (s), 15.05 (s), 13.13 (s). Anal. ($C_{21}H_{27}F_2NO_3$) calcd. % C, 66.47; H, 7.17; N, 3.69; found % C, 66.71; H, 7.02; N, 3.77. HRMS (Q-TOF) Calcd for ($C_{21}H_{27}F_2NO_3$): $[M+H]^+$ m/z: 380.2032, found 380.2037; $[M+Na]^+$ m/z: 402.1851, found 402.1851.

1-(3-Fluorophenyl)-*N*-methylmethanamine hydrochloride 8a. Method B: prepared from 2.0 N methylamine in THF (30 mmol, 15 mL) and 3-fluorobenzylbromide (3.0 mmol, 0.40 mL). The compound was transformed into the corresponding hydrochloride salt by dissolving the solid free base in the minimum volume of 1,4-dioxane before adding 4.0 N HCl in 1,4-dioxane. The resulting precipitate was collected by filtration and washed with dry dioxane, yielding **8a**. Yield: 49%. ^{1}H NMR (500 MHz, DMSO-d_6) δ: 9.08 (br s, 2H), 7.51 – 7.47 (m, 1H), 7.40 – 7.38 (m, 1H), 7.35 – 7.33 (m, 1H), 7.28 – 7.24 (m, 1H), 4.13 (s, 2H), 2.53 (s, 3H).

***N*-(3-Fluorobenzyl)ethanamine 8b.** Method B: prepared from aq. 66% w/v ethylamine (30 mmol, 2.0 mL) and 3-fluorobenzylbromide (1.5 mmol, 0.18 mL). Yield: 53%. ^{1}H NMR (300 MHz, DMSO-d_6) δ: ^{1}H NMR (300 MHz, DMSO-d_6) δ 7.43 – 7.26 (m, 1H), 7.19 – 7.06 (m, 2H), 7.06 – 6.91 (m, 1H), 3.66 (s, 2H), 2.47 (q, *J* = 7.1 Hz, 2H), 0.99 (t, *J* = 7.1 Hz, 3H), NH not detected.

***N*-(3-Fluorobenzyl)propan-2-amine 8c.** Method B: prepared from isopropylamine (30 mmol, 2.6 mL) and 3-fluorobenzylbromide (1.5 mmol, 0.18 mL). Yield: 42%. ^{1}H NMR (300 MHz, DMSO-d_6) δ: 7.37 – 7.23 (m, 1H), 7.19 – 7.09 (m, 2H), 7.06 – 6.91 (m, 1H), 3.67 (s, 2H), 2.65 (h, *J* = 6.2 Hz, 1H), 1.96 (s, 1H), 0.96 (d, *J* = 6.2 Hz, 6H).

7-{3-[Ethyl(3-fluorobenzyl)amino]propoxy}-3,4-dimethyl-2*H*-chromen-2-one 10. Method C: prepared from **8b** (0.40 mmol, 0.060 g). Yield: 80%; yellow solid; mp: 65-67 °C. ^{1}H NMR (300 MHz, DMSO-d_6) δ: 7.65 (d, *J* = 9.1 Hz, 1H), 7.33 – 7.23 (m, 1H), 7.15 – 7.04 (m, 2H), 7.03 – 6.93

(m, 1H), 6.89 – 6.81 (m, 2H), 4.06 (t, *J* = 6.4 Hz, 2H), 3.54 (s, 2H), 2.53 (d, *J* = 6.4 Hz, 2H), 2.44 (q, *J* = 7.1 Hz, 2H), 2.35 (s, 3H), 2.06 (s, 3H), 1.85 (qn, *J* = 6.4 Hz, 2H), 0.96 (t, *J* = 7.1 Hz, 3H). ^{13}C NMR (126 MHz, $CDCl_3$) δ: 162.89 (d, *J* = 245.5 Hz), 162.46 (s), 160.92 (s), 153.52 (s), 146.22 (s), 142.55 (s), 129.55 (s), 125.15 (s), 124.07 (s), 118.81 (s), 115.34 (d, *J* = 20.0 Hz), 114.07 (s), 113.59 (d, *J* = 20.0 Hz), 112.24 (s), 101.14 (s), 66.35 (s), 57.78 (s), 49.39 (s), 47.51 (s), 26.87 (s), 15.05 (s), 13.13 (s), 11.88 (s). Anal. ($C_{23}H_{26}FNO_3$) calcd. % C, 72.04; H, 6.83; N, 3.65; found % C, 71.86; H, 6.63; N, 3.74. HRMS (Q-TOF) Calcd for ($C_{23}H_{26}FNO_3$): $[M+H]^+$ m/z: 384.1969, found 384.1980; $[M+Na]^+$ m/z: 406.1789, found 406.1806.

7-{3-[(3-Fluorobenzyl)(isopropyl)amino]propoxy}-3,4-dimethyl-2*H*-chromen-2-one 11. Method C: prepared from **8c** (0.40 mmol, 0.067 g). Yield: 30%; white solid; mp: 101-102 °C. ^{1}H NMR (300 MHz, DMSO-d_6) δ: 7.65 (d, *J* = 9.5 Hz, 1H), 7.32 – 7.22 (m, 1H), 7.16 – 7.05 (m, 2H), 6.99 – 6.90 (m, 1H), 6.87 – 6.79 (m, 2H), 4.04 (t, *J* = 6.3 Hz, 2H), 3.54 (s, 2H), 2.83 (heptet, *J* = 6.5 Hz, 1H), 2.54 (t, *J* = 6.3 Hz, 2H), 2.35 (s, 3H), 2.06 (s, 3H), 1.77 (qn, *J* = 6.3 Hz, 2H), 0.95 (d, *J* = 6.5 Hz, 6H). ^{13}C NMR (126 MHz, $CDCl_3$) δ 162.93 (d, J_{CF} = 244.6 Hz), 162.49 (s), 161.01 (s), 153.52 (s), 146.25 (s), 144.17 (d, J_{CF} = 6.9 Hz), 129.46 (d, J_{CF} = 8.2 Hz), 125.10 (s), 123.70 (d, J_{CF} = 2.4 Hz), 118.72 (s), 114.96 (d, J_{CF} = 21.3 Hz), 113.98 (s), 113.38 (d, J_{CF} = 21.4 Hz), 112.26 (s), 101.09 (s), 66.24 (s), 53.74 (s), 49.73 (s), 45.55 (s), 27.94 (s), 17.82 (s), 15.04 (s), 13.12 (s). Anal. ($C_{24}H_{28}FNO_3$) calcd. % C, 72.52; H, 7.10; N, 3.52; found % C, 72.13; H, 6.96; N, 3.52. HRMS (Q-TOF) Calcd for ($C_{24}H_{28}FNO_3$): $[M+H]^+$ m/z: 398.2126, found 398.2134; $[M+Na]^+$ m/z: 420.1945, found 420.1959.

4-(Hydroxymethyl)-7-({4-[(methylamino)methyl]benzyl}oxy)-2*H*-chromen-2-one 12a. Method D: prepared from **9b** (0.50 mmol, 0.19 g). Purification procedure: column chromatography (gradient eluent: methanol in dichloromethane, 10% → 20%). Yield: 75%; yellow solid. ^{1}H NMR (300 MHz, DMSO-d_6) δ: 7.61 (d, J = 8.8 Hz, 1H), 7.53 (d, J = 8.3 Hz, 2H), 7.49 (d, J = 8.3 Hz, 2H), 7.06 (d, J = 2.4 Hz, 1H), 6.99 (dd, J = 8.8, 2.4 Hz, 1H), 6.29 (s, 1H), 5.61 (t, J = 5.5 Hz, 1H), 5.25 (s, 2H), 4.71 (d, J = 5.5 Hz, 2H), 4.11 (s, 2H), 2.54 (s, 3H), NH not detected.

3,4-Dimethyl-7-({3-[(methylamino)methyl]benzyl}oxy)-2*H*-chromen-2-one 12b. Method D: prepared from **9c** (0.50 mmol, 0.16 g). Purification procedure: column chromatography (gradient eluent: methanol in dichloromethane, 10% → 20%). Yield: 88%; pale yellow solid. ^{1}H NMR (300 MHz, DMSO-d_6) δ: 7.70 (d, *J* = 8.6 Hz, 1H), 7.59 (s, 1H), 7.54 – 7.36 (m, 3H), 7.10 – 6.91 (m, 2H), 5.20 (s, 2H), 4.06 (s, 2H), 2.50 (s, 3H), 2.35 (s, 3H), 2.09 (s, 3H).

3,4-Dimethyl-7-({4-[(methylamino)methyl]benzyl}oxy)-2*H*-chromen-2-one 12c. Method D: prepared from **9d** (0.50 mmol, 0.19 g). Purified through washing several times the crude solid with Et_2O (3.5 mL) and a mixture of Et_2O/*n*-hexane (4.5/0.5 v/v) until disappearance of impurities TLC spots. Yield: 93%; white solid. ^{1}H NMR (300 MHz, DMSO-d_6) δ: 7.69 (d, J = 9.1 Hz, 1H), 7.47 (d, J = 8.2 Hz, 2H), 7.42 (d, J = 8.2 Hz, 2H), 7.05 – 6.95 (m, 2H), 5.20 (s, 2H), 3.90 (s, 2H), 2.41 (s, 3H), 2.36 (s, 3H), 2.35 (s, 3H).

7-[(3-{[(4,4-Difluorobutyl)(methyl)amino]methyl}benzyl)oxy]-3,4-dimethyl-2*H*-chromen-2-one 13. Method E: prepared from **12b** (0.24 mmol, 0.079 g). Purification procedure: column chromatography (gradient eluent: methanol in dichloromethane, 1% → 2%). Yield: 42%; off-white solid; mp: 73-75 °C. ^{1}H NMR (500 MHz, $CDCl_3$) δ: 7.50 (d, J = 8.9 Hz, 1H), 7.40 (s, 1H), 7.38 – 7.28 (m, 3H), 6.92 (dd, J = 8.9, 2.5 Hz, 1H), 6.86 (d, J = 2.5 Hz, 1H), 5.83 (tt, J = 57.0, 4.4 Hz, 1H), 5.11 (s, 2H), 3.55 (s, 2H), 2.44 (t, J = 6.3 Hz, 2H), 2.36 (s, 3H), 2.22 (s, 3H), 2.18 (s, 3H), 1.93 – 1.81 (m, 2H), 1.73 – 1.64 (m, 2H). ^{13}C NMR (126 MHz, $CDCl_3$) δ: 162.41 (s), 160.53 (s), 153.43 (s), 146.24 (s), 139.12 (s), 136.11 (s), 128.98 (s), 128.73 (s), 128.09 (s), 126.41 (s), 125.29 (s), 119.03 (s), 117.26 (t, J = 238.7 Hz), 114.36 (s), 112.73 (s), 101.58 (s), 70.31 (s), 62.03 (s), 56.17 (s), 41.84 (s), 31.82 (t, J = 21.0 Hz), 19.73 (s), 15.08 (s), 13.16 (s). Anal. ($C_{24}H_{27}F_2NO_3$) calcd. % C, 69.38; H, 6.55; N, 3.37; found % C, 69.54; H, 6.61; N, 3.32. HRMS (Q-TOF) Calcd for ($C_{24}H_{27}F_2NO_3$): $[M+H]^+$ m/z: 416.2032, found 416.2040; $[M+Na]^+$ m/z: 438.1851, found 438.1862.

7-[(4-{[(4,4-Difluorobutyl)(methyl)amino]methyl}benzyl)oxy]-3,4-dimethyl-2*H*-chromen-2-one 14. Method E: prepared from **12c** (0.24 mmol, 0.79 g). Purification procedure: column chromatography (gradient eluent: methanol in dichloromethane, 1% → 2%). Yield: 45%; off-white solid; mp: 67-69 °C. ^{1}H NMR (300 MHz, $CDCl_3$) δ: 7.50 (d, *J* = 8.8 Hz, 1H), 7.39 (d, *J* = 8.1 Hz, 2H), 7.34 (d, *J* = 8.1 Hz, 2H), 6.92 (dd, *J* = 8.8, 2.5 Hz, 1H), 6.87 (d, *J* = 2.5 Hz, 1H), 5.83 (tt, *J* = 56.9, 4.3 Hz, 1H), 5.10 (s, 2H), 3.52 (s, 2H), 2.43 (br s, 2H), 2.37 (s, 3H), 2.21 (s, 3H), 2.18 (s, 3H), 2.00 – 1.74 (m, 2H), 1.76 – 1.62 (m, 2H). ^{13}C NMR (126 MHz, $CDCl_3$) δ: 162.38 (s), 160.52 (s), 153.46 (s), 146.17 (s), 135.19 (s), 129.50 (s), 127.83 (s), 127.76 (s), 125.27 (s), 119.07 (s), 117.15 (t, J = 239.2 Hz), 114.39 (s), 112.71 (s), 101.61 (s), 70.14 (s), 61.67 (s), 56.05 (s), 41.57 (s), 31.77 (t, J = 21.0 Hz), 19.56 (s), 15.05 (s), 13.13 (s). Anal. ($C_{24}H_{27}F_2NO_3$) calcd. % C, 69.38; H, 6.55; N, 3.37; found % C, 69.70; H, 6.48; N, 3.41. HRMS (Q-TOF) Calcd for ($C_{24}H_{27}F_2NO_3$): $[M+H]^+$ m/z: 416.2032, found 416.2030; $[M+Na]^+$ m/z: 438.1851, found 438.1851.

7-[(4-{[(4,4-Difluorobutyl)(methyl)amino]methyl}benzyl)oxy]-4-(hydroxymethyl)-2*H*-chromen-2-one 15. Method E: prepared from **12a** (0.24 mmol, 0.076 g). Purification procedure:

column chromatography (gradient eluent: methanol in dichloromethane, 1% → 5%). Yield: 50%; glass solid. ^{1}H NMR (300 MHz, $CDCl_3$) δ: 7.42 (d, *J* = 9.2 Hz, 1H), 7.38 (d, *J* = 8.3 Hz, 2H), 7.33 (d, *J* = 8.3 Hz, 2H), 6.98 – 6.86 (m, 2H), 6.46 (s, 1H), 5.83 (tt, *J* = 57.0, 4.4 Hz, 1H), 5.11 (s, 2H), 4.87 (s, 2H), 3.51 (s, 2H), 2.42 (t, *J* = 7.0 Hz, 3H), 2.20 (s, 3H), 2.03 – 1.44 (m, 4H). ^{13}C NMR (126 MHz, $CDCl_3$) δ: 161.64 (s), 161.58 (s), 155.24 (s), 154.52 (s), 137.60 (s), 135.01 (s), 129.62 (s), 127.62 (s, J = 34.5 Hz), 124.43 (s), 117.13 (t, J = 238.9 Hz), 113.11 (s), 111.14 (s), 108.87 (s), 102.02 (s), 70.17 (s), 61.63 (s), 60.68 (s), 56.08 (s), 41.59 (s), 31.75 (t, J = 21.1 Hz), 19.44 (s). Anal. ($C_{23}H_{25}F_2NO_4$) calcd. % C, 66.18; H, 6.04; N, 3.36; found % C, 66.32; H, 5.97; N, 3.30. HRMS (Q-TOF) Calcd for ($C_{23}H_{25}F_2NO_4$): $[M+H]^+$ m/z: 418.1824, found 418.1824; $[M+Na]^+$ m/z: 440.1644, found 440.1645.

7-[(4-{[(3-Fluorobenzyl)(methyl)amino]methyl}benzyl)oxy]-4-(hydroxymethyl)-2*H*-chromen-2-one hydrochloride 16. In a pyrex vessel charged with a magnetic stirring bar, intermediate **9b** (0.40 mmol, 0.15 g) was suspended in acetone (10 mL), followed by the addition of K_2CO_3 (1.6 mmol, 0.220 g), **8a** (0.80 mmol, 0.11 g), and a catalytic amount of KI. The reaction was kept under microwave irradiation for 30 min at 130 °C. After cooling to room temperature, the solid residue was filtered-off and thoroughly washed with $CHCl_3$. The resulting solution was concentrated under reduced pressure and purified by flash chromatography (gradient eluent: methanol in dichloromethane, 0% → 10%). The compound was transformed into the corresponding hydrochloride salt by dissolving the solid free base in the minimum volume of 1,4-dioxane before adding HCl 4.0 N in 1,4-dioxane. The resulting precipitate was collected by filtration and washed with dry dioxane, thus obtaining **16**. Yield: 61%; white solid; mp: > 230 °C. ^{1}H NMR (500 MHz, DMSO-*d*$_6$) δ: 10.37 (s, 1H), 7.63 (d, *J* = 8.8 Hz, 1H), 7.60 (d, *J* = 8.2 Hz, 2H), 7.57 (d, *J* = 8.2 Hz, 2H), 7.55 – 7.45 (m, 2H), 7.42 – 7.38 (m, 1H), 7.35 – 7.28 (m, 1H), 7.10 (d, *J* = 2.5 Hz, 1H), 7.02 (dd, *J* = 8.8, 2.5 Hz, 1H), 6.30 (s, 1H), 5.27 (s, 2H), 4.72 (s, 2H), 4.54 – 4.36 (m, 2H), 4.30 – 4.11 (m, 2H), 2.53 (d, *J* = 4.8 Hz, 3H). ^{13}C NMR (126 MHz, DMSO-*d*$_6$) δ: 162.34 (d, *J* = 244.4 Hz), 161.51 (s), 160.86 (s), 157.14 (s), 155.11 (s), 138.12 (s), 133.00 (d, *J* = 7.9 Hz), 132.15 (s), 131.25 (d, *J* = 8.3 Hz), 130.07 (s), 128.50 (s), 128.08 (d, *J* = 2.5 Hz), 125.91 (s), 118.66 (d, *J* = 22.2 Hz), 116.89 (d, *J* = 20.8 Hz), 113.09 (s), 111.37 (s), 108.01 (s), 102.20 (s), 69.75 (s), 66.78 (s), 59.49 (s), 58.39 (s), 57.94 (s). Anal. ($C_{26}H_2ClFNO_4$) calcd. % C, 66.45; H, 5.36; N, 2.98; found % C, 66.63; H, 5.59; N, 3.11. HRMS (Q-TOF) Calcd for ($C_{26}H_{24}FNO_4$): $[M+H]^+$ m/z: 434.1762, found 434.1772; $[M+Na]^+$ m/z: 456.1582, found 456.1594; $[M-H]^-$ m/z: 432.1617, found 432.1602.

7-[(4-{[Benzyl(methyl)amino]methyl}benzyl)oxy]-2-oxo-2*H*-chromene-4-carbaldehyde 18. In a flame-dried round-bottomed flask, **17**[32] (0.51 mmol, 0.21 g) was dissolved in anhydrous CH_2Cl_2 (10

mL). MnO_2 powder (10 mmol, 0.90 g) was added to the solution and the reaction mixture was stirred at room temperature for 2 h. After this period, the mixture was diluted with Et_2O (75 mL), the inorganic residue was filtered off through a pad of silica gel and carefully washed with Et_2O. The resulting solution was then concentrated under rotary evaporation affording the desired aldehyde. Yield: 64%; yellow solid. ^{1}H NMR (300 MHz, $CDCl_3$) δ: 10.06 (s, 1H), 8.49 (d, *J* = 9.0 Hz, 1H), 7.46 – 7.37 (m, 5H), 7.36 – 7.28 (m, 4H), 6.99 (dd, *J* = 9.0, 2.5 Hz, 1H), 6.93 (d, *J* = 2.5 Hz, 1H), 6.70 (s, 1H), 5.13 (s, 2H), 3.53 (s, 4H), 2.19 (s, 3H).

7-[(4-{[Benzyl(methyl)amino]methyl}benzyl)oxy]-4-(difluoromethyl)-2*H*-chromen-2-one 19. To a solution of **18** (0.27 mmol, 0.11 g) in dry CH_2Cl_2 (2 mL) at 0 °C under N_2 atmosphere was slowly dropped DAST (0.49 mmol, 0.064 mL) *via* syringe. After 10 min the reaction mixture was allowed to warm to room temperature and stirred overnight. The reaction mixture was then cooled to 0 °C with an external ice bath and carefully quenched with 10 mL of saturated aq. $NaHCO_3$. The mixture was then extracted with dichloromethane (3 x 15 mL). The collected organic layers were dried over anhydrous Na_2SO_4 and concentrated under rotatory evaporation. The crude residue was purified by column chromatography (eluent: ethyl acetate in dichloromethane 0.5 %). Yield: 16%; colorless oil. ^{1}H NMR (500 MHz, $CDCl_3$) δ: 7.61 (d, *J* = 8.9 Hz, 1H), 7.44 – 7.34 (m, 6H), 7.32 (t, *J* = 7.5 Hz, 2H), 7.25 – 7.22 (m, 1H), 6.97 (dd, *J* = 8.9, 2.5 Hz, 1H), 6.94 (d, *J* = 2.5 Hz, 1H), 6.70 (t, *J* = 53.8 Hz, 1H), 6.46 (s, 1H), 5.13 (s, 2H), 3.53 (s, 4H), 2.19 (s, 3H). ^{13}C NMR (126 MHz, $CDCl_3$) δ: 162.28 (s), 160.00 (s), 156.14 (s), 145.13 (t, *J* = 22.3 Hz), 135.22 – 133.76 (m), 129.51 (s), 129.48 (s), 129.09 (s), 128.34 (s), 127.59 (s), 127.55 (s), 127.26 (s), 125.82 (t, *J* = 1.8 Hz), 113.67 (s), 112.14 (t, *J* = 242.4 Hz), 111.80 (t, *J* = 8.8 Hz), 108.58 (s), 102.39 (s), 70.42 (s), 61.61 (s), 61.18 (s), 41.98 (s). Anal. ($C_{26}H_{23}F_2NO_3$) calcd. % C, 71.71; H, 5.32; N, 3.22; found % C, 71.55; H, 5.36; N, 3.21. HRMS (Q-TOF) Calcd for ($C_{26}H_{23}F_2NO_3$): $[M+H]^+$ m/z: 436.1719, found 436.1728; $[M+Na]^+$ m/z: 458.1538, found 458.1547.

Enzyme inhibition studies.

All enzymes and reagents were from Sigma Aldrich Italy. Experiments were performed in 96-well plate-based assays using a multiplate reader Infinite M1000 Pro (Tecan, Cernusco sul Naviglio, Italy) and were run in triplicate. 96-Well plates were purchased from Greiner Bio-One (Kremsmenster, Austria). IC_{50} values were obtained by nonlinear regression using Prism software (GraphPad Prism version 5.00 for Windows, GraphPad Software, San Diego, CA, USA). Inhibition of human recombinant AChE and horse serum BChE was determined by applying already published procedures[41] based on the Ellman's spectrophotometric assay[40], using transparent, flat-

bottomed plates. For human recombinant MAO A/B inhibition studies, the spectrofluorimetric protocol, based on the oxidative deamination of kynuramine to 4-hydroxyquinoline,[31] was performed in black, flat-bottomed plates. The same protocol was adopted for the spectrophotometric detection of 4-hydroxyquinoline (absorbance at 316 nm) in transparent, flat-bottomed plates as previously described.[18]

Supporting information

The Supporting Information is available free of charge at https://_____:

Molecular formula strings (MFS) (CSV); Protocols for early-ADME experiments (kinetic solubility, PAMPA-HDM, PAMPA-BBB, $LogD_{7.4}$, CHI, HSA binding, Caco-2 permeability, microsomal stability, Cytochrome P450 3A4 inhibition); Absorbance protocol for MAO B inhibition; Reversibility MAO B binding assays: Methods for molecular docking simulations; Cell-based assay protocols (SH-SY5Y and HepG2 cytotoxicity, neuroprotection).

AUTHOR INFORMATION

Corresponding Author

Leonardo Pisani – Department of Pharmacy-Drug Sciences, University of Bari "Aldo Moro", via Orabona 4, 70125-Bari, Italy; orcid.org/0000-0002-4198-3897; Phone: +39-0805442803; Fax: +39-080-5442230; E-mail: leonardo.pisani@uniba.it.

Notes

The authors declare no competing financial interest.

ABBREVIATIONS

AChE, acetylcholinesterase; AD, Alzheimer's disease; BBB, blood brain barrier; BChE, butyrylcholinesterase; CAS, catalytic anionic subsite; CNS, central nervous system; CHI, chromatographic hydrophobicity index; CL_{int}, intrinsic clearance; DAST, (diethylamino)sulfur

trifluoride; ER, efflux ratio; HDM, hexadecane membrane; HSA, human serum albumin; MAO, monoamine oxidase; MTT, 3-(4,5-dimethylthiazol-2-yl)-2,5-diphenyl-tetrazolium bromide; ND, neurodegenerative disease; NMDA, N-methyl-D-aspartate; P_{app}, apparent permeability; PAMPA, parallel artificial membrane permeability assay; PAS, peripheral anionic subsite; PBLE, porcine brain lipid extracts; PBS, phosphate buffered saline; PCC, pyridinium chlorochromate; P-gp, P-glycoprotein; Q-TOF, Quadrupole Time-of-Flight; ROS, reactive oxygen species; RP-HPLC, reversed-phase high-performance liquid chromatography; SAR, structure-activity relationships; SPR, surface plasmon resonance; TEER, trans-epithelial electrical resistance; TLC, thin layer chromatography.

References

(1) 2020 Alzheimer's Disease Facts and Figures. *Alzheimer's Dement.* **2020**, *16* (3), 391–460.

(2) Saez-Atienzar, S.; Masliah, E. Cellular Senescence and Alzheimer Disease: The Egg and the Chicken Scenario. *Nat. Rev. Neurosci.* **2020**, *21* (8), 433–444.

(3) Dubois, B.; Hospital, D.; Dubois, B.; Feldman, H. H.; Jacova, C.; rey Cummings, J. L.; DeKosky, S. T.; Barberger-Gateau, P.; Delacourte, A.; Frisoni, G.; Fox, N. C.; Galasko, D.; Gauthier, S.; Hampel, H.; Jicha, G. A.; Meguro, K.; Pasquier, F.; Robert, P.; Rossor, M.; Salloway, S.; Sarazin, M.; de Souza, L. C.; Stern, Y.; Visser, P. J.; Scheltens, P. Position Paper Revising the Defi Nition of Alzheimer's Disease: A New Lexicon. *Lancet Neurol.* **2010**, *9*, 1118–1127.

(4) Querfurth, H. W.; LaFerla, F. M. Alzheimer's Disease: Mechanism of Disease. *N. Engl. J. Med.* **2010**, *362* (4), 329–344.

(5) Domingo-Fernández, D.; Kodamullil, A. T.; Iyappan, A.; Naz, M.; Emon, M. A.; Raschka, T.; Karki, R.; Springstubbe, S.; Ebeling, C.; Hofmann-Apitius, M. Multimodal Mechanistic Signatures for Neurodegenerative Diseases (NeuroMMSig): A Web Server for Mechanism Enrichment. *Bioinformatics* **2017**, *33* (22), 3679–3681.

(6) Citron, M. Alzheimer's Disease: Strategies for Disease Modification. *Nat. Rev. Drug Discov.* **2010**, *9* (5), 387–398.

(7) Wang, H.; Zhang, H. Reconsideration of Anticholinesterase Therapeutic Strategies against Alzheimer's Disease. *ACS Chem. Neurosci.* **2019**, *10* (2), 852–862.

(8) Mangialasche, F.; Solomon, A.; Winblad, B.; Mecocci, P.; Kivipelto, M. Alzheimer's Disease: Clinical Trials and Drug Development. *Lancet. Neurol.* **2010**, *9* (7), 702–716.

(9) Cummings, J. L.; Morstorf, T.; Zhong, K. Alzheimer's Disease Drug-Development Pipeline: Few Candidates, Frequent Failures. *Alzheimer's Res. Ther.* **2014**, *6* (4).

(10) Cummings, J.; Lee, G.; Ritter, A.; Sabbagh, M.; Zhong, K. Alzheimer's Disease Drug Development Pipeline: 2020. *Alzheimer's Dement. Transl. Res. Clin. Interv.* **2020**, *6* (1).

(11) León, R.; Garcia, A. G.; Marco-Contelles, J. Recent Advances in the Multitarget-Directed Ligands Approach for the Treatment of Alzheimer's Disease. *Med. Res. Rev.* **2013**, *33* (1), 139–189.

(12) Lecoutey, C.; Hedou, D.; Freret, T.; Giannoni, P.; Gaven, F.; Since, M.; Bouet, V.; Ballandonne, C.; Corvaisier, S.; Malzert Freon, A.; Mignani, S.; Cresteil, T.; Boulouard, M.; Claeysen, S.; Rochais, C.; Dallemagne, P. Design of Donecopride, a Dual Serotonin Subtype 4 Receptor Agonist/Acetylcholinesterase Inhibitor with Potential Interest for Alzheimer's Disease Treatment. *Proc. Natl. Acad. Sci.* **2014**, *111* (36), E3825–E3830.

(13) Malek, R.; Arribas, R. L.; Palomino-Antolin, A.; Totoson, P.; Demougeot, C.; Kobrlova, T.; Soukup, O.; Iriepa, I.; Moraleda, I.; Diez-Iriepa, D.; Godyń, J.; Panek, D.; Malawska, B.; Głuch-Lutwin, M.; Mordyl, B.; Siwek, A.; Chabchoub, F.; Marco-Contelles, J.; Kiec-Kononowicz, K.; Egea, J.; de los Ríos, C.; Ismaili, L. New Dual Small Molecules for Alzheimer's Disease Therapy Combining Histamine H 3 Receptor (H3R) Antagonism and Calcium Channels Blockade with Additional Cholinesterase Inhibition. *J. Med. Chem.* **2019**, *62* (24), 11416–11422.

(14) Oukoloff, K.; Coquelle, N.; Bartolini, M.; Naldi, M.; Le Guevel, R.; Bach, S.; Josselin, B.; Ruchaud, S.; Catto, M.; Pisani, L.; Denora, N.; Iacobazzi, R. M.; Silman, I.; Sussman, J. L.; Buron, F.; Colletier, J.-P.; Jean, L.; Routier, S.; Renard, P.-Y. Design, Biological Evaluation and X-Ray Crystallography of Nanomolar Multifunctional Ligands Targeting Simultaneously Acetylcholinesterase and Glycogen Synthase Kinase-3. *Eur. J. Med. Chem.* **2019**, *168*, 58–77.

(15) Simoni, E.; Daniele, S.; Bottegoni, G.; Pizzirani, D.; Trincavelli, M. L.; Goldoni, L.; Tarozzo, G.; Reggiani, A.; Martini, C.; Piomelli, D.; Melchiorre, C.; Rosini, M.; Cavalli, A. Combining Galantamine and Memantine in Multitargeted, New Chemical Entities Potentially Useful in Alzheimer's Disease. *J. Med. Chem.* **2012**, *55* (22), 9708–9721.

(16) Brunschweiger, A.; Koch, P.; Schlenk, M.; Pineda, F.; Küppers, P.; Hinz, S.; Köse, M.; Ullrich, S.; Hockemeyer, J.; Wiese, M.; Heer, J.; Müller, C. E. 8-Benzyltetrahydropyrazino[2,1-f]Purinediones: Water-Soluble Tricyclic Xanthine Derivatives as Multitarget Drugs for Neurodegenerative Diseases. *ChemMedChem* **2014**, *9* (8), 1704–1724.

(17) Bautista-Aguilera, Ó. M.; Hagenow, S.; Palomino-Antolin, A.; Farré-Alins, V.; Ismaili, L.; Joffrin, P.-L.; Jimeno, M. L.; Soukup, O.; Janočková, J.; Kalinowsky, L.; Proschak, E.; Iriepa, I.; Moraleda, I.; Schwed, J. S.; Romero Martínez, A.; López-Muñoz, F.; Chioua, M.; Egea, J.; Ramsay, R. R.; Marco-Contelles, J.; Stark, H. Multitarget-Directed Ligands Combining Cholinesterase and Monoamine Oxidase Inhibition with Histamine H3 R Antagonism for Neurodegenerative Diseases. *Angew. Chem. Int. Ed. Engl.* **2017**, *56* (41), 12765–12769.

(18) Pisani, L.; Iacobazzi, R. M.; Catto, M.; Rullo, M.; Farina, R.; Denora, N.; Cellamare, S.; Altomare, C. D. Investigating Alkyl Nitrates as Nitric Oxide Releasing Precursors of Multitarget Acetylcholinesterase-Monoamine Oxidase B Inhibitors. *Eur. J. Med. Chem.* **2019**, *161*, 292–309.

(19) Rullo, M.; Catto, M.; Carrieri, A.; de Candia, M.; Altomare, C. D.; Pisani, L. Chasing ChEs-MAO B Multi-Targeting 4-Aminomethyl-7-Benzyloxy-2H-Chromen-2-Ones. *Molecules*

2019, *24* (24), 4507.

(20) Košak, U.; Strašek, N.; Knez, D.; Jukič, M.; Žakelj, S.; Zahirović, A.; Pišlar, A.; Brazzolotto, X.; Nachon, F.; Kos, J.; Gobec, S. N-Alkylpiperidine Carbamates as Potential Anti-Alzheimer's Agents. *Eur. J. Med. Chem.* **2020**, *197*, 112282.

(21) He, Q.; Liu, J.; Lan, J.-S.; Ding, J.; Sun, Y.; Fang, Y.; Jiang, N.; Yang, Z.; Sun, L.; Jin, Y.; Xie, S.-S. Coumarin-Dithiocarbamate Hybrids as Novel Multitarget AChE and MAO-B Inhibitors against Alzheimer's Disease: Design, Synthesis and Biological Evaluation. *Bioorg. Chem.* **2018**, *81*, 512–528.

(22) Reis, J.; Cagide, F.; Valencia, M. E.; Teixeira, J.; Bagetta, D.; Pérez, C.; Uriarte, E.; Oliveira, P. J.; Ortuso, F.; Alcaro, S.; Rodríguez-Franco, M. I.; Borges, F. Multi-Target-Directed Ligands for Alzheimer's Disease: Discovery of Chromone-Based Monoamine Oxidase/Cholinesterase Inhibitors. *Eur. J. Med. Chem.* **2018**, *158*, 781–800.

(23) Kumar, B.; Dwivedi, A. R.; Sarkar, B.; Gupta, S. K.; Krishnamurthy, S.; Mantha, A. K.; Parkash, J.; Kumar, V. 4,6-Diphenylpyrimidine Derivatives as Dual Inhibitors of Monoamine Oxidase and Acetylcholinesterase for the Treatment of Alzheimer's Disease. *ACS Chem. Neurosci.* **2019**, *10* (1), 252–265.

(24) Xu, Y.; Zhang, J.; Wang, H.; Mao, F.; Bao, K.; Liu, W.; Zhu, J.; Li, X.; Zhang, H.; Li, J. Rational Design of Novel Selective Dual-Target Inhibitors of Acetylcholinesterase and Monoamine Oxidase B as Potential Anti-Alzheimer's Disease Agents. *ACS Chem. Neurosci.* **2019**, *10* (1), 482–496.

(25) Weinreb, O.; Amit, T.; Bar-Am, O.; Youdim, M. B. H. Ladostigil: A Novel Multimodal Neuroprotective Drug with Cholinesterase and Brain-Selective Monoamine Oxidase Inhibitory Activities for Alzheimer's Disease Treatment. *Curr. Drug Targets* **2012**, *13* (4), 483–494.

(26) Schneider, L. S.; Geffen, Y.; Rabinowitz, J.; Thomas, R. G.; Schmidt, R.; Ropele, S.; Weinstock, M.; Ladostigil Study Group. Low-Dose Ladostigil for Mild Cognitive Impairment: A Phase 2 Placebo-Controlled Clinical Trial. *Neurology* **2019**, *93* (15), e1474–e1484.

(27) Inestrosa, N. C.; Dinamarca, M. C.; Alvarez, A. Amyloid-Cholinesterase Interactions: Implications for Alzheimer's Disease. *FEBS J.* **2008**, *275* (4), 625–632.

(28) Kim, D.; Hoon Baik, S.; Kang, S.; Won Cho, S.; Bae, J.; Cha, M.-Y.; J. Sailor, M.; Mook-Jung, I.; Han Ahn, K. Close Correlation of Monoamine Oxidase Activity with Progress of Alzheimer's Disease in Mice, Observed by in Vivo Two-Photon Imaging. *ACS Cent. Sci.* **2016**, *2* (12), 967–975.

(29) Gulyás, B.; Pavlova, E.; Kása, P.; Gulya, K.; Bakota, L.; Várszegi, S.; Keller, É.; Horváth, M. C.; Nag, S.; Hermecz, I.; Magyar, K.; Halldin, C. Activated MAO-B in the Brain of Alzheimer Patients, Demonstrated by [11C]-l-Deprenyl Using Whole Hemisphere Autoradiography. *Neurochem. Int.* **2011**, *58* (1), 60–68.

(30) Saura, J.; Luque, J. M.; Cesura, A. M.; Prada, M. Da; Chan-Palay, V.; Huber, G.; Löffler, J.; Richards, J. G. Increased Monoamine Oxidase b Activity in Plaque-Associated Astrocytes of Alzheimer Brains Revealed by Quantitative Enzyme Radioautography. *Neuroscience* **1994**, *62* (1), 15–30.

(31) Pisani, L.; Farina, R.; Catto, M.; Iacobazzi, R. M.; Nicolotti, O.; Cellamare, S.; Mangiatordi,

G. F.; Denora, N.; Soto-Otero, R. R.; Siragusa, L.; Altomare, C. D.; Carotti, A. Exploring Basic Tail Modifications of Coumarin-Based Dual Acetylcholinesterase-Monoamine Oxidase B Inhibitors: Identification of Water-Soluble, Brain-Permeant Neuroprotective Multitarget Agents. *J. Med. Chem.* **2016**, *59* (14), 6791–6806.

(32) Farina, R.; Pisani, L.; Catto, M.; Nicolotti, O.; Gadaleta, D.; Denora, N.; Soto-Otero, R.; Mendez-Alvarez, E.; Passos, C. S.; Muncipinto, G.; Altomare, C. D.; Nurisso, A.; Carrupt, P.-A.; Carotti, A. Structure-Based Design and Optimization of Multitarget-Directed 2 H - Chromen-2-One Derivatives as Potent Inhibitors of Monoamine Oxidase B and Cholinesterases. *J. Med. Chem.* **2015**, *58* (14), 5561–5578.

(33) Hagmann, W. K. The Many Roles for Fluorine in Medicinal Chemistry. *J. Med. Chem.* **2008**, *51* (15), 4359–4369.

(34) Böhm, H.-J.; Banner, D.; Bendels, S.; Kansy, M.; Kuhn, B.; Müller, K.; Obst-Sander, U.; Stahl, M. Fluorine in Medicinal Chemistry. *Chembiochem* **2004**, *5* (5), 637–643.

(35) Meanwell, N. A. Fluorine and Fluorinated Motifs in the Design and Application of Bioisosteres for Drug Design. *J. Med. Chem.* **2018**, *61* (14), 5822–5880.

(36) Gillis, E. P.; Eastman, K. J.; Hill, M. D.; Donnelly, D. J.; Meanwell, N. A. Applications of Fluorine in Medicinal Chemistry. *J. Med. Chem.* **2015**, *58* (21), 8315–8359.

(37) Zafrani, Y.; Sod-Moriah, G.; Yeffet, D.; Berliner, A.; Amir, D.; Marciano, D.; Elias, S.; Katalan, S.; Ashkenazi, N.; Madmon, M.; Gershonov, E.; Saphier, S. CF2H, a Functional Group-Dependent Hydrogen-Bond Donor: Is It a More or Less Lipophilic Bioisostere of OH, SH, and CH3? *J. Med. Chem.* **2019**, *62* (11), 5628–5637.

(38) Zafrani, Y.; Yeffet, D.; Sod-Moriah, G.; Berliner, A.; Amir, D.; Marciano, D.; Gershonov, E.; Saphier, S. Difluoromethyl Bioisostere: Examining the "Lipophilic Hydrogen Bond Donor" Concept. *J. Med. Chem.* **2017**, *60* (2), 797–804.

(39) Vorberg, R.; Trapp, N.; Zimmerli, D.; Wagner, B.; Fischer, H.; Kratochwil, N. A.; Kansy, M.; Carreira, E. M.; Müller, K. Effect of Partially Fluorinated N -Alkyl-Substituted Piperidine-2-Carboxamides on Pharmacologically Relevant Properties. *ChemMedChem* **2016**, *11* (19), 2216–2239.

(40) Ellman, G. L.; Courtney, K. D.; Andres, V.; Featherstone, R. M. A New and Rapid Colorimetric Determination of Acetylcholinesterase Activity. *Biochem. Pharmacol.* **1961**, *7* (2), 88–90.

(41) Pisani, L.; Catto, M.; De Palma, A.; Farina, R.; Cellamare, S.; Altomare, C. D. Discovery of Potent Dual Binding Site Acetylcholinesterase Inhibitors via Homo- and Heterodimerization of Coumarin-Based Moieties. *ChemMedChem* **2017**, *12* (16), 1349–1358.

(42) Blackwelll, B.; Mabbitt, L. A. Tyramine in Cheese Related to Hypertensive Crises After Monoamine-Oxidase Inihibition. *Lancet (London, England)* **1965**, *1* (7392), 938–940.

(43) Purgatorio, R.; de Candia, M.; Catto, M.; Carrieri, A.; Pisani, L.; De Palma, A.; Toma, M.; Ivanova, O. A. O. A.; Voskressensky, L. G. L. G.; Altomare, C. D. C. D. Investigating 1,2,3,4,5,6-Hexahydroazepino[4,3-b]Indole as Scaffold of Butyrylcholinesterase-Selective Inhibitors with Additional Neuroprotective Activities for Alzheimer's Disease. *Eur. J. Med. Chem.* **2019**, *177*, 414–424.

(44) Sterling, T.; Irwin, J. J. ZINC 15 – Ligand Discovery for Everyone. *J. Chem. Inf. Model.*

2015, *55* (11), 2324–2337.

(45) Baell, J. B.; Holloway, G. A. New Substructure Filters for Removal of Pan Assay Interference Compounds (PAINS) from Screening Libraries and for Their Exclusion in Bioassays. *J. Med. Chem.* **2010**, *53* (7), 2719–2740.

(46) Lagorce, D.; Sperandio, O.; Baell, J. B.; Miteva, M. A.; Villoutreix, B. O. FAF-Drugs3: A Web Server for Compound Property Calculation and Chemical Library Design. *Nucleic Acids Res.* **2015**, *43* (W1), W200-7.

(47) Aldrich, C.; Bertozzi, C.; Georg, G. I.; Kiessling, L.; Lindsley, C.; Liotta, D.; Merz, K. M.; Schepartz, A.; Wang, S. The Ecstasy and Agony of Assay Interference Compounds. *J. Med. Chem.* **2017**, *60* (6), 2165–2168.

(48) Valkó, K.; Bevan, C.; Reynolds, D. Chromatographic Hydrophobicity Index by Fast-Gradient RP-HPLC: A High-Throughput Alternative to Log P/Log D. *Anal. Chem.* **1997**, *69* (11), 2022–2029.

(49) Wager, T. T.; Chandrasekaran, R. Y.; Hou, X.; Troutman, M. D.; Verhoest, P. R.; Villalobos, A.; Will, Y. Defining Desirable Central Nervous System Drug Space through the Alignment of Molecular Properties, in Vitro ADME, and Safety Attributes. *ACS Chem. Neurosci.* **2010**, *1* (6), 420–434.

(50) Purgatorio, R.; Candia, M.; Catto, M.; Rullo, M.; Pisani, L.; Denora, N.; Carrieri, A.; Nevskaya, A. A.; Voskressensky, L. G.; Altomare, C. D. Evaluation of Water-Soluble Mannich Base Prodrugs of 2,3,4,5-Tetrahydroazepino[4,3- b]Indol-1(6 H)-one as Multitarget-Directed Agents for Alzheimer's Disease. *ChemMedChem* **2021**, *16* (3), 589–598.

(51) Rich, R. L.; Day, Y. S. N.; Morton, T. A.; Myszka, D. G. High-Resolution and High-Throughput Protocols for Measuring Drug/Human Serum Albumin Interactions Using BIACORE. *Anal. Biochem.* **2001**, *296* (2), 197–207.

(52) Frostell-Karlsson, Å.; Remaeus, A.; Roos, H.; Andersson, K.; Borg, P.; Hämäläinen, M.; Karlsson, R. Biosensor Analysis of the Interaction between Immobilized Human Serum Albumin and Drug Compounds for Prediction of Human Serum Albumin Binding Levels. *J. Med. Chem.* **2000**, *43* (10), 1986–1992.

(53) Pisani, L.; Catto, M.; Giangreco, I.; Leonetti, F.; Nicolotti, O.; Stefanachi, A.; Cellamare, S.; Carotti, A. Design, Synthesis, and Biological Evaluation of Coumarin Derivatives Tethered to an Edrophonium-like Fragment as Highly Potent and Selective Dual Binding Site Acetylcholinesterase Inhibitors. *ChemMedChem* **2010**, *5* (9), 1616–1630.

(54) Pisani, L.; Rullo, M.; Catto, M.; de Candia, M.; Carrieri, A.; Cellamare, S.; Altomare, C. D. Structure-Property Relationship Study of the HPLC Enantioselective Retention of Neuroprotective 7-[(1-Alkylpiperidin-3-Yl)Methoxy]Coumarin Derivatives on an Amylose-Based Chiral Stationary Phase. *J. Sep. Sci.* **2018**, *41* (6), 1376–1384.

(55) Rullo, M.; Niso, M.; Pisani, L.; Carrieri, A.; Colabufo, N. A.; Cellamare, S.; Altomare, C. D. 1,2,3,4-Tetrahydroisoquinoline/2H-Chromen-2-One Conjugates as Nanomolar P-Glycoprotein Inhibitors: Molecular Determinants for Affinity and Selectivity over Multidrug Resistance Associated Protein 1. *Eur. J. Med. Chem.* **2019**, *161*, 433–444.

Table of Contents Graphic